TECHNICAL REPORT BRL-TR-2915

BRL

1938 – Serving the Army for Fifty Years – 1988

NUMERICAL SIMULATION OF UNSTEADY INCOMPRESSIBLE FLOW IN A PARTIALLY-FILLED ROTATING CYLINDER

MICHAEL J. NUSCA

JUNE 1988

U.S. ARMY LABORATORY COMMAND

BALLISTIC RESEARCH LABORATORY

ABERDEEN PROVING GROUND, MARYLAND

DESTRUCTION NOTICE

Destroy this report when it is no Ionger needed. DO NOT return it to the originator.

Additional copies of this report may be obtained from the National Technical Information Service, U.S. Department of Commerce, Springfield, VA 22161.

The findings of this report are not to be construed as an official Department of the Army position, unless so designated by other authorized documents.

The use of trade names or manufacturers' names in this report does not constitute indorsement of any commercial product.

8c. ADDRESS (City, State, and ZIP Code)	10. SOURCE OF FUNDING NUMBERS			
	PROGRAM ELEMENT NO.	PROJECT NO.	TASK NO.	WORK UNIT ACCESSION N
Aberdeen Proving Ground, MD 21005-5066	62618A	1L1 62618AH80		

11. TITLE (*Include Security Classification*)

Numerical Simulation of Unsteady Incompressible Flow in a Partially-Filled Rotating Cylin

12. PERSONAL AUTHOR(S)

Nusca, Michael J.

13a. TYPE OF REPORT	13b. TIME COVERED	14. DATE OF REPORT (*Year, Month, Day*)	15. PAGE COUNT
Technical Report	FROM _____ TO _____	1988 Jun	50

16. SUPPLEMENTARY NOTATION

17. COSATI CODES			18. SUBJECT TERMS (*Continue on reverse if necessary and identify by block number*)
FIELD	GROUP	SUB-GROUP	
01	01		Finite Difference, Liquid Moment,
			Incompressible Flow, Unsteady Flow,
19	06		Liquid-Filled Projectile, Rotating Liquids,

19. ABSTRACT (*Continue on reverse if necessary and identify by block number*)

The liquid flowfield in a full or partially-filled right circular cylinder in rapid axial rotation is investigated numerically. The governing equations are the axisymmetric, unsteady, viscous, incompressible Navier-Stokes equations. These equations are written in stream function-vorticity form for a cylindrical coordinate system in a nonrotating reference frame. The governing equations are discretized using second-order finite-differences for time and space on a nonuniform grid employing logarithmic stretching in regions where high flow gradients are anticipated. Time dependent solutions for Reynolds numbers betwe 1,000 and 100,000 have been obtained using a Gauss-Seidel relaxation procedure. For parti ly filled cases the free surface is assumed to be cylindrical and located at a constant radius from the axis of spin. Numerical solutions for full cylinders are consistent with previous solutions and experimental data. Numerical solutions for a partially-filled cyl der are consistent with experimental data for a liquid centrifuge except at the free surf Computations of the roll moment exerted on the cylinder by the contained liquid shows a smaller moment for the partially-filled compared with the full cylinder results.

20. DISTRIBUTION / AVAILABILITY OF ABSTRACT	21. ABSTRACT SECURITY CLASSIFICATION	
☐ UNCLASSIFIED/UNLIMITED ☒ SAME AS RPT ☐ DTIC USERS	UNCLASSIFIED	
22a. NAME OF RESPONSIBLE INDIVIDUAL	22b. TELEPHONE (*Include Area Code*)	22c. OFFICE SYMBOL
Michael J. Nusca	(301)-278-2057	SLCBR-LF-A

Acknowledgement

The following individuals have contributed to the completion of this work: Dr. William P. D'Amico, Dr. Gene Cooper, and Mr. Nathan Gerber of the Launch and Flight Division, U.S. Army Ballistic Research Laboratory, Aberdeen Proving Ground, Maryland. Dr. Sukumar Chakravarthy of Rockwell International Science Center, Thousand Oaks, California, provided technical guidance in the implementation of the numerical solution scheme for the equations of motion. This work was completed in partial fulfillment of a Master of Science degree at the University of Maryland; Dr. John D. Anderson, advisor.

Table of Contents

List of Figures

List of Figures (Continued)

I. INTRODUCTION

The objective of this work was to investigate the axisymmetric, unsteady, viscous, incompressible liquid flow in a rapidly rotating right circular cylinder. Understanding of this internal flow is necessary in the design of gun-launched projectiles which carry liquid payloads. Liquid-filled projectiles exhibit flight instabilities that are not observed for the same vehicle with a rigid payload. These instabilities have been described by Stewartson.[1] The Stewartson principle states that resonance between the inertial wave frequency in the rotating liquid and the nutation frequency of the projectile can cause projectile instability. A numerical procedure for solving the unsteady Navier-Stokes equations was developed for the present study. From a computational viewpoint, this problem is instructive since it represents a class of internal flow problems for which computational experiments can reveal details of the flow that cannot be easily measured experimentally. This study of axisymmetric free surface flow represents the initial stage of an investigation of the three-dimensional problem.

Theoretical and experimental work examining the flow within a rotating cylinder has concentrated on full cylinders.[2] Experimental evidence[3] indicates that the effect of a free surface on enclosed rotating liquids is important. Particular interests include shear layers that may form on the liquid-air interface, the role of liquid viscosity and interior flow circulation in restoring the disturbed fluid to a state of rigid body rotation, the pressure and shear forces exerted on the cylinder walls by the liquid, and the resulting liquid roll moment on the container.

Computational work for this problem has taken several forms. Kitchens[4] adapted a predictor-corrector, multiple-iteration scheme, which was developed by Rubin and Lin[5] for steady flows, combined with a Gauss-Seidel iteration scheme to solve the time-dependent flow in a cylinder spinning up from rest. Chakravarthy[6] composed two time accurate schemes to compute the time-dependent flow for the spin-up problem. In one scheme the finite-differenced equations in primitive variable form were solved using an implicit approximate factorization procedure. The second scheme solved the equations in stream function-vorticity form using a Gauss-Seidel relaxation procedure. Kitchens and Chakravarthy produced comparable results for filled cylinders. Homicz and Gerber[7] extended a model by Goller and Ranov[8] and produced a finite-difference scheme for spin-up from rest in a partially-filled rotating cylinder. This analysis assumed columnar flow (i.e. flow velocities and pressure are independent of the axial coordinate) and thus the azimuthal momentum equation was the sole equation considered. This equation was solved using an implicit Crank-Nicolson scheme.

Shadday[9] conducted an experimental and numerical investigation of the internal flowfield of a liquid centrifuge. He considered a partially-filled right circular cylinder in rapid rotation with the internal flowfield induced by the differential rotation of one endwall with respect to the rest of the container. Shadday gathered axial and azimuthal velocity data along radii of the cylinder using a laser-Doppler velocimeter (LDV). In addition, a numerical scheme was formulated in primitive variables and used a modified marker-and-cell (MAC) implicit scheme. This scheme included an explicit treatment of the governing equations with the exception of the Coriolis acceleration terms. The numerical study used

a coarse grid in the radial direction. An inadequate correlation between numerical and experimental data at the liquid free surface was noted.

The aim of the present numerical investigation was to simulate the time dependent liquid flow in a closed, partially-filled cylindrical container. The spinrate of the cylinder was sufficiently large so that the liquid free surface was also cylindrical and centered on the spin axis. In this state the fluid was considered to be in solid body rotation. The spinrate was then perturbed by an instantaneous acceleration to a new steady spin resulting in a time dependent response of the fluid to the change in rotation of the cylinder. The partially-filled cylinder problem had two special requirements. The computational grid had to be sufficient to resolve a possible free surface shear layer, as well as, boundary layers on the solid walls of the container (sidewall and endwalls). In addition, the boundary conditions on the free surface had to be posed in a compatible way with the numerical framework.

In this study the Navier-Stokes equations were written in cylindrical coordinates. Since the symmetry axis of the cylindrical container was identical to the spin axis of the system, the formulation was written assuming an axisymmetric flowfield. The Navier-Stokes equations were written in stream function-vorticity form. This choice permits solution of the equations using standard methods without the use of artificial compressibility.

The method of artificial compressibility was developed by Chorin[10] to solve the primitive variable formulation of the incompressible Navier-Stokes equations. In this form an inherent numerical difficulty is created due to the absence of a time derivative in the continuity equation. To facilitate the construction of an implicit, approximately factored numerical method, a fictitious time-dependent term, designed to vanish as steady state is approached, is used to modify the continuity equation. However, approximately factorized schemes incur errors due to the factorization. When this type of scheme is combined with the artificial compressibility terms in the continuity equation, the momentum equations are then contaminated by this factorization error.

The choice of nonprimitive variables allows the solution of the governing equations without augmentation with artificial terms. The Navier-Stokes equations were discretized on a grid utilizing logarithmic stretching to cluster grid points near solid boundaries and the free surface. Second-order finite-differences were used for all derivative terms in the governing equations except the convection terms for which upwind differencing was employed. Finally, the equations are numerically relaxed using a Gauss-Seidel iteration method.

II. FREE SURFACE CONSTRAINTS

For this numerical investigation the angular velocity of the cylinder is considered to be large enough that the fluid forms an annulus of near uniform thickness on the vertical wall. The following conditions are assumed:

1. Initially, the container is rotating with spin rate Ω_i and the fluid is in a state of rigid-body rotation (i.e. the azimuthal component of velocity is directly proportional to radial position, $V = \Omega_i R$ and all other components of velocity are zero).

2. The free surface is cylindrical and centered on the spin axis. This implies that the radial acceleration is much greater than the gravitational acceleration (g), or the Froude number, $\mathrm{Fr} = \Omega_i^2 a/g \gg 1$ for a cylinder of radius a. This constraint on Ω_i results in a Froude number that is larger than the Ekman number, $E = \nu/\Omega_i c^2$ where c is the cylinder half-height and ν is the kinematic viscosity of the liquid.

Winch[11] and Gerber[12] derived a set of equations that describe the shape of the free surface in a partially-filled cylinder in steady state axial rotation. These equations verify that a chosen set of conditions (Fr, cylinder aspect ratio and fill ratio) will result in a vertical free surface. For a right circular cylinder that is partially-filled with liquid and that is suddenly rotated at a constant angular velocity Ω_f, the fluid will rise along the sidewall of the cylinder and form a parabolic free surface. When the fluid finally attains the angular velocity of the cylinder, a steady state or equilibrium shape is reached and is defined by:

$$Z = Z_o + \frac{\Omega_f^2 R^2}{2g} \tag{1}$$

Equation 1 describes a parabola with a vertex that intersects the spin axis of the cylinder at a height of Z_o. Using Equation (1) and conservation of liquid mass, Gerber[12] has derived an equation for the shape of the free surface when the free surface intersects both endwalls of the cylinder:

$$Z = \frac{\Omega_f^2 a^2}{4cg} Z_i + c + \frac{\Omega_f^2}{2g}\left(R^2 - a^2\right) \tag{2}$$

where c is the cylinder half-height, a is the radius, and Z_i is the initial ($\Omega_f = 0$) liquid level in the cylinder.

Nondimensionalizing $z = Z/a$ and $r = R/a$ and defining the fill ratio, $f = Z_i/(2c)$, and aspect ratio, $\alpha = c/a$, we write Equation (2) as,

$$z = \alpha + \frac{\mathrm{Fr}}{2\alpha}\left(r^2 - 1 + f\right) \tag{3}$$

When the free surface intersects both the bottom wall ($z = 0$) and the top wall ($z = 2\alpha$) of the cylinder, we can define the radial location of the free surface at $z = 0$,

$$r_1 = \left[1 - f - \frac{2\alpha}{\mathrm{Fr}}\right]^{1/2} \tag{4}$$

and the radial location of the free surface at $z = 2\alpha$,

$$r_2 = \left[1 - f + \frac{2\alpha}{\mathrm{Fr}}\right]^{1/2} \tag{5}$$

For a given set of parameters ($f = 0.95, \alpha = 3.0$), Figure 1 shows the difference in free surface radial location between the cylinder endwalls ($r_2 - r_1$) as a function of Froude number. The free surface first intersects both end walls at about $\mathrm{Fr} = 109$.

The free surface is essentially vertical for Fr above 900. For this Fr ($a = 0.1$ meters), $\Omega_f^2 a = 8829$ meters/sec^2 $\gg g = 9.81$ meters/sec^2 and the slope of the free surface is nearly infinite. An equation for the radial location of the free surface can be derived from conservation of liquid mass[13], or by setting Fr $= \infty$ in Equation (4) or (5).

$$r_i = (1 - f)^{1/2} \tag{6}$$

where $r_i = 0.2236$ for the parameters specified above.

III. GOVERNING EQUATIONS

The motion of fluid within a rotating cylinder is governed by the unsteady, incompressible Navier-Stokes equations. The natural coordinate system for this problem is the cylindrical system (r, θ, z) where $u, v,$ and w are the radial, azimuthal, and axial velocity components respectively. Disturbances to the motion of the cylindrical container are axisymmetric, thus, the flowfield is axisymmetric. The equations are written in axisymmetric form by eliminating all θ derivatives. The dimensionless form of the equations in the nonrotating reference frame are;

Continuity equation

$$\frac{1}{r}\frac{\partial(ru)}{\partial r} + \frac{\partial w}{\partial z} = 0 \tag{7}$$

Momentum equations

$$\frac{\partial u}{\partial \tau} + u\frac{\partial u}{\partial r} + w\frac{\partial u}{\partial z} - \frac{v^2}{r} = -\frac{\partial p}{\partial r} + \frac{1}{\mathrm{Re}}\left(\frac{\partial^2 u}{\partial r^2} + \frac{1}{r}\frac{\partial u}{\partial r} + \frac{\partial^2 u}{\partial z^2} - \frac{u}{r^2}\right) \tag{8}$$

$$\frac{\partial v}{\partial \tau} + u\frac{\partial v}{\partial r} + w\frac{\partial v}{\partial z} + \frac{uv}{r} = \frac{1}{\mathrm{Re}}\left(\frac{\partial^2 v}{\partial r^2} + \frac{1}{r}\frac{\partial v}{\partial r} + \frac{\partial^2 v}{\partial z^2} - \frac{v}{r^2}\right) \tag{9}$$

$$\frac{\partial w}{\partial \tau} + u\frac{\partial w}{\partial r} + w\frac{\partial w}{\partial z} = -\frac{\partial p}{\partial z} + \frac{1}{\mathrm{Re}}\left(\frac{\partial^2 w}{\partial r^2} + \frac{1}{r}\frac{\partial w}{\partial r} + \frac{\partial^2 w}{\partial z^2}\right) \tag{10}$$

where,

$r = R/a, \quad z = Z/a, \quad u = U/\Omega_f a, \quad v = V/\Omega_f a, \quad w = W/\Omega_f a$
$p = P/\rho\Omega_f^2 a^2, \quad \tau = T\Omega_f, \quad \mathrm{Re} = \Omega_f a^2/\nu$

The stream function-vorticity form of the Navier-Stokes equations is used in the solution scheme. The definition of these variables are:

$$\text{Stream function} \quad \psi_z = ru \tag{11}$$

$$\psi_r = -rw \tag{12}$$

$$\text{Vorticity} \quad \zeta = u_z - w_r \tag{13}$$

$$\text{Circulation} \quad \gamma = rv \tag{14}$$

The governing equations cast in this form are obtained as follows. The first equation of the new system is derived from the definition of vorticity (Eq. 13) using the definition of stream function (Eqs. 11,12). This equation is elliptic and is in the form of a Poisson equation. The radial momentum equation (Eq. 8) is differentiated with respect to z and from this equation the r derivative of the axial momentum equation (Eq. 10) is subtracted. This cross-differentiation eliminates pressure and yields a parabolic vorticity transport equation. The azimuthal momentum equation (Eq. 9) is recast into a parabolic equation using the definition of circulation (Eq. 14). The stream function-vorticity form of the Navier-Stokes equations are:

$$\frac{\partial^2\psi}{\partial r^2} + \frac{\partial^2\psi}{\partial z^2} - \frac{1}{r}\frac{\partial\psi}{\partial r} = r\zeta \tag{15}$$

$$\frac{\partial\zeta}{\partial\tau} + u\frac{\partial\zeta}{\partial r} + w\frac{\partial\zeta}{\partial z} - \frac{u}{r}\zeta - \frac{2\gamma}{r^3}\frac{\partial\gamma}{\partial z} = \frac{1}{\mathrm{Re}}\left(\frac{\partial^2\zeta}{\partial r^2} + \frac{\partial^2\zeta}{\partial z^2} + \frac{1}{r}\frac{\partial\zeta}{\partial r} - \frac{\zeta}{r^2}\right) \tag{16}$$

and the circulation equation is:

$$\frac{\partial\gamma}{\partial\tau} + u\frac{\partial\gamma}{\partial r} + w\frac{\partial\gamma}{\partial z} = \frac{1}{\mathrm{Re}}\left(\frac{\partial^2\gamma}{\partial r^2} + \frac{\partial^2\gamma}{\partial z^2} - \frac{1}{r}\frac{\partial\gamma}{\partial r}\right) \tag{17}$$

Equation 16 is nonlinear in the convective terms $\left(\frac{\partial\zeta}{\partial r} + w\frac{\partial\zeta}{\partial z}\right)$ since u and w are functions of the dependent variable ζ via Equation 13. The equation is parabolic in time and poses an initial value problem. The same is true of the circulation equation (Eq. 17). The stream function equation (Eq. 15) is elliptic and poses a boundary value problem which can be solved by iterative methods. Equation 15 is de-coupled from the vorticity equation (Eq. 16) and the circulation equation (Eq. 17). As a result, Equations 16 and 17 can be solved first, followed by the separate solution of Equation 15 with vorticity as a source term.

IV. BOUNDARY CONDITIONS

The governing equations are applied to the domain of interest as shown in Figure 2. In the case of a cylinder full of liquid the boundaries of the domain are the endwalls ($Z = 0$ and $Z = 2c$), the sidewall ($R = a$) and the geometric axis ($R = 0$) about which the cylinder spins. For the partially-filled cylinder, the boundary at $R = 0$ is replaced by a free surface located at $R = R_i$. The location of the free surface was discussed in Section II and given by Equation 6. The boundary conditions for the free surface will be discussed later in this section.

The governing equations are written in the inertial (nonrotating) reference frame, thus, the no-slip boundary conditions on the cylinder walls are: $U = W = 0, V = \Omega_f a$ for $R = a$; $U = W = 0, V = \Omega_f R$ for $Z = 0$; and $U = W = 0, V = \Omega_f R$ for $Z = 2c$. These no-slip boundary conditions are made dimensionless using the same definitions employed for the governing equations and become:

$$r = 1 : u = w = 0, v = 1 \tag{18}$$

$$z = 0 : u = w = 0, v = r \tag{19}$$

$$z = 2\alpha : u = w = 0, v = r \tag{20}$$

The boundary conditions for the cylinder axis are derived from the nondimensional continuity equation in primitive variable form (Eq. 7):

$$\frac{1}{r}\frac{\partial(ru)}{\partial r} + \frac{\partial w}{\partial z} = 0 \quad \text{or} \quad r\frac{\partial u}{\partial r} + u + r\frac{\partial w}{\partial z} = 0 \tag{21}$$

Now, setting $r = 0$, we obtain $u = 0$. Multiplying both sides of the axial momentum equation (Eq. 10) by r and setting $r = 0$ we obtain the condition $\partial w/\partial r = 0$. Multiplying both sides of the azimuthal momentum equation (Eq. 9) by r^2 and setting $r = 0$ we obtain the condition $v = 0$. Hence,

$$r = 0 : u = v = 0, \frac{\partial w}{\partial r} = 0 \tag{22}$$

Because of flow symmetry we restrict the domain bounded by $0 \le r \le 1$, $0 \le z \le 2\alpha$ to a computational domain bounded by $0 \le r \le 1, 0 \le z \le \alpha$ (Figure 2). In Reference 13, computational verification of flow symmetry was performed over the domain $z = 0$ to 2α for a cylinder full of liquid. We term this situation the "gyroscope problem" since the entire cylinder undergoes the same motion. Once the flowfield for $0 \le r \le 1, 0 \le z \le \alpha$ (one quadrant) is computed, the flowfield in the rest of the cylinder can be obtained. This domain restriction creates an additional boundary, the symmetry plane, requiring a boundary condition. On the symmetry plane we require no axial flow and no axial flow gradients for the radial and azimuthal velocity components. Thus,

$$z = \alpha : w = 0, \frac{\partial u}{\partial z} = 0, \frac{\partial v}{\partial z} = 0 \tag{23}$$

The above restriction of the domain using symmetry arguments does not apply when different parts of the cylinder have different angular velocities as in the "centrifuge problem". In this case, the bottom wall and the side wall of the cylinder have an angular velocity, Ω_f, that is not the same as the angular velocity of the top wall, Ω_f'. As a result two quadrants ($0 \le r \le 1, 0 \le z \le 2\alpha$) of the flowfield must be considered as the flow is symmetric about the spin axis but not the midplane of the cylinder. This adds the boundary condition:

$$z = 2\alpha : u = w = 0, v = \frac{\Omega_f'}{\Omega_f} r \tag{24}$$

The boundary conditions are written in the variables of stream function, vorticity, and circulation. For the gyroscope problem the conversion of boundary conditions to the nonprimitive variables is as follows:

Axis: $(r = 0)$	$r = 0$	with Equations 11 and 12 yields:	$\psi = 0$
	$u = w_r = 0$	with Equation 13 yields:	$\zeta = 0$
	$v = 0$	with Equation 14 yields:	$\gamma = 0$

$$\psi = 0, \qquad \zeta = 0, \qquad \gamma = 0 \tag{25}$$

Sidewall: $(r = 1)$	$u = w = 0$	with Equations 11 and 12 yields:	$\psi = 0$
	$u_z = 0$	with Equation 13 yields:	$\zeta = -w_r = \psi_{rr}$
	$v = 1$	with Equation 14 yields:	$\gamma = 1$

$$\psi = 0, \qquad \zeta = \psi_{rr}, \qquad \gamma = 1 \tag{26}$$

Endwall: $(z = 0)$	$u = w = 0$	with Equations 11 and 12 yields:	$\psi = 0$
	$w_r = 0$	with Equation 13 yields:	$\zeta = u_z = \frac{1}{r}\psi_{zz}$
	$v = r$	with Equation 14 yields:	$\gamma = r^2$

$$\psi = 0, \qquad \zeta = \frac{1}{r}\psi_{zz}, \qquad \gamma = r^2 \tag{27}$$

Symmetry Plane: $(z = \alpha)$	$w = 0$	with Equations 11 and 12 yields:	$\psi = 0$
	$u_z = w = 0$	with Equation 13 yields:	$\zeta = 0$
	$v_z = 0$	with Equation 14 yields:	$\gamma_z = 0$

$$\psi = 0, \qquad \zeta = 0, \qquad \gamma_z = 0 \tag{28}$$

For the centrifuge problem the fluid is driven by the top wall of the cylindrical container. This top wall has a steady spinrate that is not the same as the spinrate for the rest of the cylinder. As noted in the derivation of the governing equations, the spinrate used to yield dimensionless equations is Ω_f. The boundary condition on the symmetry plane (Eq. 28) is replaced by:

$$\text{Endwall } (z = 2\alpha): \quad \psi = 0, \qquad \zeta = \frac{1}{r}\psi_{zz}, \qquad \gamma = \frac{\Omega_f'}{\Omega_f} r^2 \tag{29}$$

The free surface boundary conditions on γ and ζ can be derived from the assumption that the free surface does not support tangential stress (i.e. $\tau_{\theta r} = \tau_{zr} = 0$).

$$\tau_{\theta r} = \frac{\mu}{2}\left[r\frac{\partial(v/r)}{\partial r} + \frac{1}{r}\frac{\partial u}{\partial \theta}\right] = \frac{\mu}{2}\left[r\frac{\partial(vr/r^2)}{\partial r}\right] = \frac{\mu}{2}\left[\frac{\partial(\gamma/r^2)}{\partial r}\right] = 0 \text{ or } \frac{\partial(\gamma/r^2)}{\partial r} = 0 \tag{30}$$

$$\tau_{zr} = \frac{\mu}{2}\left[\frac{\partial u}{\partial z} + \frac{\partial w}{\partial r}\right] = \frac{\mu}{2}\left[-\frac{\partial u}{\partial z} + \frac{\partial w}{\partial r} + 2\frac{\partial u}{\partial z}\right] = \frac{\mu}{2}\left[-\zeta + \frac{2}{r}\psi_{zz}\right] = 0 \quad \text{or} \quad 2\psi_{zz} - r\zeta = 0 \tag{31}$$

Since the stream-function equation (Eq. 15) is elliptic and its solution represents a boundary value problem, the boundary condition for stream function on the free surface should be a Dirichlet or Neumann condition. Since the condition $\psi = 0$ is imposed on the other boundaries (endwalls and sidewall) of the cylinder, the Dirichlet condition $\psi = 0$ is also imposed on the free surface. This condition is equivalent to setting $u = 0$ on the free surface and is consistent with the vertical free surface assumption made in Section II. As a result, the free surface is characterized as a "slippery rod" of radius r_i. The free surface ($r = r_i$) boundary conditions are prescribed as:

$$\psi = 0, \qquad \zeta = 0, \qquad \frac{\partial}{\partial r}\left(\frac{\gamma}{r^2}\right) = 0 \tag{32}$$

From Equation 32, values of γ on the free surface can be obtained from values of γ in the interior flow using a second order forward finite-difference in the radial direction. Use of Equation 32 as boundary conditions for the free surface is restrictive. Surface waves and free surface shape changes are ignored. Unfortunately, these phenomena have been shown to exist for rotating and nutating free surface flows. Stewartson[1], in predicting the flow in a partially-filled cylinder, derived a free surface boundary condition which included small perturbations to the free surface shape ($r_i + \eta$). In the present formulation, Stewartson's condition yields a time-dependent boundary condition for ψ on the free surface. However, since Equation 15 consists of only spatial derivatives in ψ, the boundary condition on ψ cannot be time-dependent. Therefore, Stewartson's condition cannot be used with the incompressible Navier-Stokes equations in stream function-vorticity form.

Free surface boundary conditions such as Equation 32 were used by Harlow and Welch[14] in a paper that described the marker and cell method. In this work the marker and cell technique was applied to the time-dependent flow of an incompressible fluid, the boundary of which was partially confined and partially free. The time-dependent Navier-Stokes equations were written in primitive variable form and free surface boundary conditions were required for all variables. Velocity boundary conditions at a free surface were derived from the continuity equation while the pressure boundary condition was based on a constant external (or applied) pressure. They observed that the pressure condition should be based on the requirement of vanishing normal stress component at the free surface, but this would be difficult to implement unless the orientation of the surface was known at all times. They observed that such a determination was unreasonably difficult for a finite-difference scheme (assuming an Eulerian approach) and equated the pressure on the free surface to the applied pressure. Harlow and Welch achieved remarkably accurate results for a wide class of free surface problems in uncontained, nonrotating flow systems.

V. NUMERICAL SOLUTION SCHEME

This section gives the numerical solution scheme for the governing equations with the boundary conditions presented in preceding sections. First an overview of the solution

methodology is presented which is similar to those used in previous references.[15,16,17,18] The computational domain for the gyroscope problem is bounded by one cylinder endwall, the symmetry plane, the cylinder sidewall and the free surface (Figure 2). For the centrifuge problem the domain is bounded by the cylinder endwalls, the cylinder sidewall and the free surface. A grid is constructed in the domain, and the solution is computed at mesh points on the grid. The computation begins with initial values for $\psi, \zeta, \gamma, u, v,$ and w at every mesh point and at time equal to zero. For a time accurate solution where transient flow phenomenon are of interest, the initial solution corresponds to a real flow condition:

$$\psi = 0, \quad \zeta = 0, \quad \gamma = \frac{\Omega_i}{\Omega_f} r^2, \quad u = 0, \quad v = \frac{\Omega_i}{\Omega_f} r, \quad w = 0 \tag{33}$$

At time level $\tau = \tau + \Delta\tau$, the computational cycle begins with the simultaneous solution of the finite-difference analog of Equations 16 and 17 for ζ and γ at all interior mesh points. The governing equations are discretized directly on a stretched grid. This procedure has been used by other researchers[6]. The next step is to solve the finite-difference analog of Equation 15 at all interior mesh points. This equation involves computed values of ζ as a source term. These equations are solved by Gauss-Seidel relaxation using successive over-relaxation (SOR). At this point new velocity components are evaluated from the definitions of stream function (Equations 11 and 12) and circulation (Equation 13). Finally, the boundary conditions are imposed. Iterative solution of the flowfield for the current time step is continued until convergence. The computational cycle is repeated until the desired time is reached.

Stretching of the grid in the computational domain is accomplished with the following equation (after Roberts[19]):

$$r = \frac{d\{[(d+1)/(d-1)]^{\beta} - 1\}}{1 + [(d+1)/(d-1)]^{\beta}} \tag{34}$$

where a uniformly spaced coordinate, $\beta(x)$, can be transformed into a nonuniform coordinate, $r(x)$, that varies continuously throughout the domain but is clustered near the boundaries.[19] The parameter $d < 1$ is the control to achieve desired clustering with very fine boundary spacing for $d \ll 1$. Similarly for the axial direction, a uniformly spaced coordinate, $\eta(x)$, can be transformed into a nonuniform coordinate, $z(x)$, using:

$$z = \frac{\alpha(1 - b + (1+b)[(b+1)/(b-1)]^{\eta-1})}{1 + [(b+1)/(b-1)]^{\eta-1}} \tag{35}$$

The parameter $b < 1$ is defined in the same manner as d. These formulas are derived in Reference 13. For a full cylinder, grid points are clustered at $R = a$ and $Z = 0$. For a partially-filled cylinder, grid points are clustered at $R = a$, $R = R_i$ and $Z = 0$. Figures 3 and 4 show typical grids for the full and partially-filled cases ($c/a = 1.0$).

The finite-difference analog of the governing equations[13] are obtained using central and upwind difference expressions for the derivative terms. The convective terms of Equations 16 and 17 are represented using upwind differencing (see Appendix C, Reference 13). All other derivative terms are represented using central differences. All spatial derivatives are represented by three-point second order finite-difference formula. The time derivative is represented by a second order difference formula.

The iterative solution of the governing equations is accomplished using Gauss-Seidel relaxation.[17,20] Gauss-Seidel iterations converge very rapidly provided that a condition of diagonal dominance exists for the coefficient matrix of the system of equations. For the governing equations formulated in stream function, vorticity and circulation variables, diagonal dominance has been shown to exist.[15] The present study uses a modification of the Gauss-Seidel method called successive over-relaxation (SOR). This technique accelerates the convergence of the algorithm and as a result reduces the required computational time. As the Gauss-Seidel iteration is applied to the system of simultaneous algebraic equations several iterations are made before convergence to an acceptable level is achieved. During this process we observe the direction of the change in the unknown at a grid point between two successive iterations and anticipate that the same trend will continue on to the next iteration. To accelerate convergence, an arbitrary correction to the intermediate values of the unknown is made:

$$u_{ij}^{k+1'} = u_{ij}^{k'} + \omega \left(u_{ij}^{k+1} - u_{ij}^{k'} \right) \tag{36}$$

Here, k denotes iteration level and u_{ij}^{k+1} is the most recent value of u_{ij} calculated from the Gauss-Seidel procedure, $u_{ij}^{k'}$ is the value from the previous iteration as adjusted by previous application of this formula, and $u_{ij}^{k+1'}$ is the guess for u_{ij} at the $k+1$ iteration level. The formula is applied immediately at each point after u_{ij}^{k+1} has been obtained and $u_{ij}^{k+1'}$ replaces u_{ij}^{k+1} in all subsequent calculations in the cycle. The relaxation parameter is ω. For over-relaxation $1 < \omega < 2$. For convergence $\omega \leq 2$. In the present study a constant value of 1.75 was used.

VI. COMPARISONS WITH PREVIOUS WORK

The computational scheme is initially checked for accuracy by comparison with flow velocity data from experiments with a filled right circular cylinder. Watkins and Hussey[21] used LDV to measure the azimuthal velocity component in a cylinder of aspect ratio unity, spinning up to an angular rate of 1.83 radians per second from rest. The Reynolds number of the flow was 9741.6 based on the final spinrate of the container. Azimuthal velocity was measured radially across the midplane of the cylinder at various times in the spin-up process. This is compared to the present work in which a 31 x 31 (r, z) grid was used with logarithmic stretching in the radial ($d = 0.05$) and axial ($b = 0.05$) directions. Figure 3 illustrates the computational grid. The solution was started with the cylinder at rest and instantaneously given the spinrate of 1.83 rad/sec. This process approximates the experimental procedure in which the container required a small amount of time to achieve full rotational speed. Watkins and Hussey recorded velocity profile measurements at various time intervals between 42.8 and 210 seconds during the spin-up process. The computation used a small numerical time step (0.0183 seconds) to insure numerical stability and was checked at 45, 75, 105 and 150 seconds in the spin-up calculation. Figure 5 shows a comparison between the measured and computed azimuthal velocity profile across the midplane of the cylinder at these times. In addition, the solution by Kitchens[4] is shown. In all cases the comparison to measured azimuthal velocity is good. Completion of the spin-up process is observed after 150 seconds as the azimuthal velocity profile takes on a linear behavior ($V = \Omega_f R$).

A second experimental case by Watkins and Hussey provides an additional comparison between the numerical code and LDV measurements for a cylinder full of liquid. For this case the aspect ratio of the cylinder was increased to 1.515 and the Reynolds number was decreased to 3076. The identical grid and logarithmic stretching constants were used. Again the cylinder was initially at rest and was instantly given an axial spinrate of 1.34 radians per second. The computational time step was again chosen as 0.0183 seconds and the computation was checked at 15, 45, 75, and 120 seconds. Figure 6 shows good comparisons between measured and computed azimuthal velocity profiles on the midplane of the cylinder. For this case the smaller Reynolds number indicates a shorter spin-up time and this is indeed observed.

A third computation is compared to the solution of the von Karman problem. This is the steady flow of an incompressible viscous liquid due to an infinite rotating disk. A stationary liquid occupies the semi-infinite region on one side of the disk, the motion of which is rotationally symmetric. The effect of the disk is to move the fluid near its surface radially outwards, and in turn induce an axial flow. The main interest in this problem is that, by virtue of assumptions about the velocity components, the Navier-Stokes equations reduce to a set of ordinary, nonlinear differential equations in a single independent variable. Several papers have been devoted to the solution of this set of equations, including Rogers and Lance[22].

For a cylinder of aspect ratio unity, initially at rest and instantaneously accelerated to an axial spinrate of 1.83 radians per second, the resulting Reynolds number is 9741.6. Early in the spin-up process the core flow is not rotating (azimuthal velocity is zero), and only the fluid near the endwalls and sidewall is effected by the container's motion. The present computation was performed using a time step of 0.0055 seconds and marched to a time of 4.54 seconds. Figure 7 shows the azimuthal velocity profile very near the endwall ($Z/a = 0.092$) and approximately outside the Ekman layer (for this case the Ekman layer thickness is of order 0.01 or $E^{1/2}$). Note that the flow between the cylinder axis and about $R/a = 0.82$ is not rotating. This region of fluid meets the criteria for the von Karman problem, i.e., a rotating disk beneath a fluid at rest. Figure 8 shows the radial velocity profile at a radius of $R/a = 0.76$, near the cylinder endwall and in the Ekman layer. The agreement with Rogers and Lance and the Navier-Stokes solution of Kitchens[4] is good. The radial velocity profile crosses into values less than zero at about $Z/a = 0.07$. This is generally defined as the edge of the Ekman layer because the radial velocity profile passes through zero at one axial point for a particular radial location (exceptions occur for transient reverse flow regions). The initial guess for the order of thickness for the Ekman layer (0.01) is also verified.

Another check on the computation comes from inertial oscillations which occur when the angular velocity of the cylinder is suddenly increased. These inertial oscillations are transients in the flowfield that eventually cease. Warn-Varnas et al[23] used LDV to detect the presence of these oscillations in a cylinder of aspect ratio 0.3182, full of water and disturbed from an initial state of solid body rotation at 0.6282 radians per second to a new spinrate of 0.7678 radians per second. The resulting Reynolds number of the flow (based on the final spin rate) was 7334. They collected azimuthal velocity data at several locations in the flowfield during the spin-up of the liquid. These velocity measurements

were then reduced to a nondimensional zonal velocity defined by,

$$\text{Zonal Velocity} = \Omega_f(1 - v/r)/(\Omega_f - \Omega_i) \tag{37}$$

which takes on the value of zero when the fluid has attained a new state of solid body rotation ($v = r$). The present computation was performed for this case using a 43x21 stretched grid and a time step of 0.0052 seconds. Azimuthal velocity was collected for every time step at 4 grid points, corresponding to the locations used by Warn-Varnas.

Figures 9 thru 12 show the comparisons between measured and computed zonal velocity versus time, for two axial locations at a radial location of $R/a = 0.25$ (in the core flow near the spin axis of the cylinder). Figure 9 shows an axial location of $Z/a = 0.3182$ (at the midplane of the cylinder) and Figure 10 shows an axial location of $Z/a = 0.079$ (near the cylinder endwall). The Navier-Stokes solution of Kitchens[4] is also shown in Figure 9. Correlations between computation and measurement are within the experimental accuracy reported by Warn-Varnas. These plots illustrate the axial structure of the inertial oscillations. The amplitude of the oscillations are nearly the same at both axial locations, but a phase shift has occurred. Figures 11 and 12 show the comparisons between measured and computed zonal velocity versus time for the same axial locations, but at a radial location of $R/a = 0.75$ (near the cylinder sidewall). Once again the axial structure of the inertial oscillations are observed; however, the amplitude of the oscillations is severely damped. This more gradual transition to solid body rotation may be due in part to the proximity of these points to the sidewall boundary layers.

In the case of a partially-filled cylinder, the free surface boundary conditions can be checked against available data from Shadday.[9] He measured the axial and azimuthal velocity components in a partially-filled cylinder initially in a state of solid body rotation and disturbed by the acceleration of the top wall to a new steady state spinrate. The rotation rate of the cylinder sidewall and bottom wall was maintained. For this configuration, the flow is no longer symmetric about the cylinder midplane; thus, the entire flowfield, for one azimuthal plane, must be computed.

The cylinder was 36.7% full of liquid ten times more viscous than water. In the experiment the entire cylinder was rotated at 1000 rpm until a steady state flow condition was reached. Then the top wall of the cylinder was accelerated by 5% in spinrate while the rest of the cylinder was maintained at 1000 rpm. The system was maintained until steady flow existed. Based on a spinrate of 1000 rpm, the Reynolds number was 93518.0 (the Ekman number was 1.0119×10^{-5}). The aspect ratio of the cylinder was 1.028. LDV measurements of flow velocity profiles were made radially across the flowfield at four specified heights from the bottom wall (Figure 13).

For the computation of this flowfield, the free surface was assumed to be vertical and located at a nondimensional radius of 0.7957. This radial location was measured by Shadday continuously during the test and reported to be constant. As a verification, the method described in Section II was used to check the shape of the free surface under these conditions. For the axial spinrate in this experiment, the slope of the free surface was 0.690 degrees.

The grid chosen for the computation consisted of 30 points in the radial direction and 61 points in the axial direction (Figure 14). Grid stretching was used to cluster grid points

near the solid boundaries and the free surface. The grid spacing at the cylinder sidewall and endwalls was .0014 and .0018, respectively. This results in at least 2 grid points within the wall boundary layers. The thickness of the sidewall and endwall boundary layers are $O(E^{1/4})$ and $O(E^{1/2})$, respectively. Grid clustering on the free surface was the same as that used on the cylinder sidewall. Several grid sensitivity studies were conducted to insure that the chosen grid was adequate.

The LDV measurements of radial velocity profiles were recorded by Shadday after the top wall was accelerated to a new spinrate and the resultant flow had achieved steady state. Shadday reports a predicted time of 6.0 seconds for the flow to reach steady state $((c^2/\Omega_f\nu)^{1/2})$. Shadday's time-dependent computation was run for 7.4 seconds. The current time-dependent solution was also run for 7.4 seconds and studies were made to verify that the solution had indeed reached a steady state. It was observed, however, that steady state was reached well before 6.0 seconds.

Figures 15 through 22 show the comparison between measured and computed velocity components at axial stations of $Z/a = 0.497$, 0.9, 1.304, and 1.706. In each case, the nondimensional axial and azimuthal velocity is hown as a function of radial position. Figure 13 illustrates the locations of these axial stations relative to the differentially rotating endwall. For the azimuthal velocity, the agreement between measurements and computations, using both the present code and Shadday's results, is good for all axial stations. For the axial velocity, agreement with measurements for both codes is good except near the free surface. The magnitude of this discrepancy is nearly constant for all axial stations.

The discrepancy between computed and measured axial velocity near the free surface may be due in part to a velocity bias in the LDV system, as reported by Shadday. This discrepancy may also be due to the free surface shape and boundary condition assumptions. Recall that the present work assumes that the free surface is vertical. An attempt was made to minimize this effect in the experiment by choosing an axial spinrate that yielded a free surface slant of less that a degree. In addition, the boundary conditions were obtained using the assumption of inviscid free surface flow (zero tangential shear stress) and constant normal pressure on the free surface. Although the effect of the inviscid boundary condition on the final result is not known, this boundary condition would be violated most severely near the differentially rotating endwall.

VII. RESULTS AND DISCUSSION

In this section, the resultant roll moment exerted on the cylinder is examined for full and partially-filled cylinders in rapid axial rotation. The container is initially in a state of solid body rotation with an axial spin rate that is suddenly accelerated. The parameters chosen for this study were Reynolds number 1000, cylinder aspect ratio 3.0, initial spinrate 300.0 rad/sec, final spinrate 400.0 rad/sec, cylinder radius 0.1 meters, liquid-fill density 1400 kilograms/meter^3 and liquid fill ratios of .95 and 1.0.

For both the full and partially-filled cases, a 21 x 41 grid was selected with the logarithmic grid clustering at the endwalls, sidewall and free surface. The Ekman number for

these flow conditions is 1.11×10^{-4} and provides guidance for the selection of grid clustering at the flow boundaries. For the sidewall and free surface, the grid spacing is selected as .0042 ($< E^{1/4}$). For the endwall, the grid spacing is selected as .0089 ($< E^{1/2}$). Figures 23 and 24 display the computational grids for cylinders with fill ratios of 1.0 and 0.95, respectively. The location of the free surface, $r_i = 0.2236$, was found from Equation 6. Figure 1 shows the difference in free surface radial location at $z = 6$ and $z = 0$, Δr, as a function of Froude number. For the initial spinrate of 300 rad/sec (Fr = 917.43, a = 0.1 meters), the slope of the free surface is about 0.20 degrees. The numerical computation was carried out for 1000 time steps or to 0.0025 seconds. At this time, the liquid has sufficiently adjusted to the cylinder spinrate; and the resultant liquid roll moment has been significantly reduced.

An important calculation for this problem is the roll moment exerted on the cylinder by the liquid fill. The moment is obtained by integrating the shear stress tangent to the cylinder endwalls and sidewall over the entire cylinder. The contribution to the roll moment at each grid point on the cylinder endwalls is proportional to $\tau_{z\theta}$ which for the case of axisymmetric flow is $\mu(\partial v/\partial z)$. The contribution to the roll moment at each grid point on the cylinder sidewall is proportional to $\tau_{r\theta}$ which is equal to $\mu(\partial v/\partial r - v/r)$. The roll moment is made dimensionless using a convention suggested by Murphy[24]:

$$C_{LRM} = \frac{\text{Roll Moment}}{(\text{liquid mass})(\text{cylinder radius})^2(\text{final spinrate})^2} \tag{38}$$

where the liquid mass is defined by the container volume and liquid density. The liquid roll moment is less than zero because the liquid acts to despin the container. When the liquid is in a state of solid body rotation, before the perturbation to axial spinrate and after the liquid has adjusted to the perturbation, C_{LRM} is zero. This can be used as an indication of the liquid spin-up time. Figure 25 shows the time history of the total coefficient of liquid roll moment. C_{LRM} for the partially-filled case is less than that for the full case. After a very short time, C_{LRM} approaches zero. The smaller C_{LRM} for the partially-filled cylinder suggests that either the wall shear stress is different in the partially-filled case or that the part of the cylinder endwall between $r = 0$ and $r = r_i$ for the full case is a major contributor to the total moment.

Figures 26 and 27 show the sidewall and endwall components of C_{LRM}. The sidewall contributes significantly to the total roll moment and shows a marked difference for full and partially-filled cylinders. For the cylinder endwall, difference in C_{LRM} for the partially-filled and full cases is insignificant. Figure 28 shows the azimuthal velocity profiles near the cylinder sidewall for two axial locations. These values are computed for 0.00025 seconds after the perturbation. At this time, the largest difference in C_{LRM} between the full and partially-filled cylinders is computed (see Figure 26). The sidewall component of the shear stress, and thus C_{LRM}, is proportional to the radial derivative of the azimuthal velocity $(\partial v/\partial r - v/r)$. The computed difference in this derivative for the two cylinder-fill ratios, when integrated over the entire sidewall, yields the computed difference in the values of C_{LRM}.

Figure 29 shows the relative difference in the computed C_{LRM} for the filled and partially-filled cylinders. For this plot the computation was extended to 2000 time steps or 0.005 secs. Whereas, the difference in C_{LRM} between $f = 1$ and $f = 0.95$ approaches

zero in the limit, the relative difference in C_{LRM} approaches a constant that is greater than 0.3 for this case. Since the relative difference is increasing with time, C_{LRM} for $f = 1$ is approaching zero faster than the difference in C_{LRM} for $f = 1$ and $f = 0.95$.

VIII. CONCLUSIONS

The internal liquid flowfield in a partially-filled right circular cylinder in rapid axial rotation has been investigated. Currently, Reynolds numbers up to 100,000 have been computed. The present work uses the axisymmetric Navier-Stokes equations but is restricted to spin-up of the liquid from one state of solid body rotation to another. Limits on the axial rotation rate of the container are chosen such that the shape of the free surface remains vertical. The present work uses the stream function-vorticity form of the unsteady, viscous, incompressible Navier-Stokes equations. As a result, the finite-difference analog of these equations are directly solved, using Gauss-Seidel SOR, without modification with artificial compressibility terms. Upwind differencing has been selectively employed for the convective terms of the governing equations. Logarithmic grid stretching has been employed near wall boundaries of the flow, as well as the free surface.

Verification of the spatial and temporal accuracy of the numerical scheme has been demonstrated for a rotating cylinder full of liquid. The required digital computer resources, such as run time and storage, are minimal with typical cases averaging 30 CPU minutes on a VAX 8600 mini-computer to attain steady-state solutions (in addition to the time accurate solutions saved during the run).

Free surface boundary conditions on vorticity and circulation were derived based on the assumption of zero tangential shear stress. A Dirichlet boundary condition was chosen for the stream function that was consistent with the assumption of a vertical free surface. These conditions were also employed by Shadday.[9] Both computations show an inadequate correlation with LDV measurements of the axial velocity component at the free surface. The present work employs a computational scheme based on the stream function-vorticity form of the governing equations that is very different from the scheme used by Shadday. In addition, the present work uses computational grids that are highly clustered at the boundaries of the domain. The similar results generated by these two very different computational approaches points to the free surface boundary conditions as the likely source of discrepancy. However, a possible velocity bias in the LDV measurements near the free surface was described by Shadday.

The relative importance of the free surface was investigated by comparison of a Reynolds number 1000 flow in a full and partially-filled cylinder during spin-up from one state of solid body rotation to another. The sidewall component of the liquid roll moment for the partially-filled cylinder differed significantly from that of the cylinder full of liquid. The endwall component was virtually unchanged.

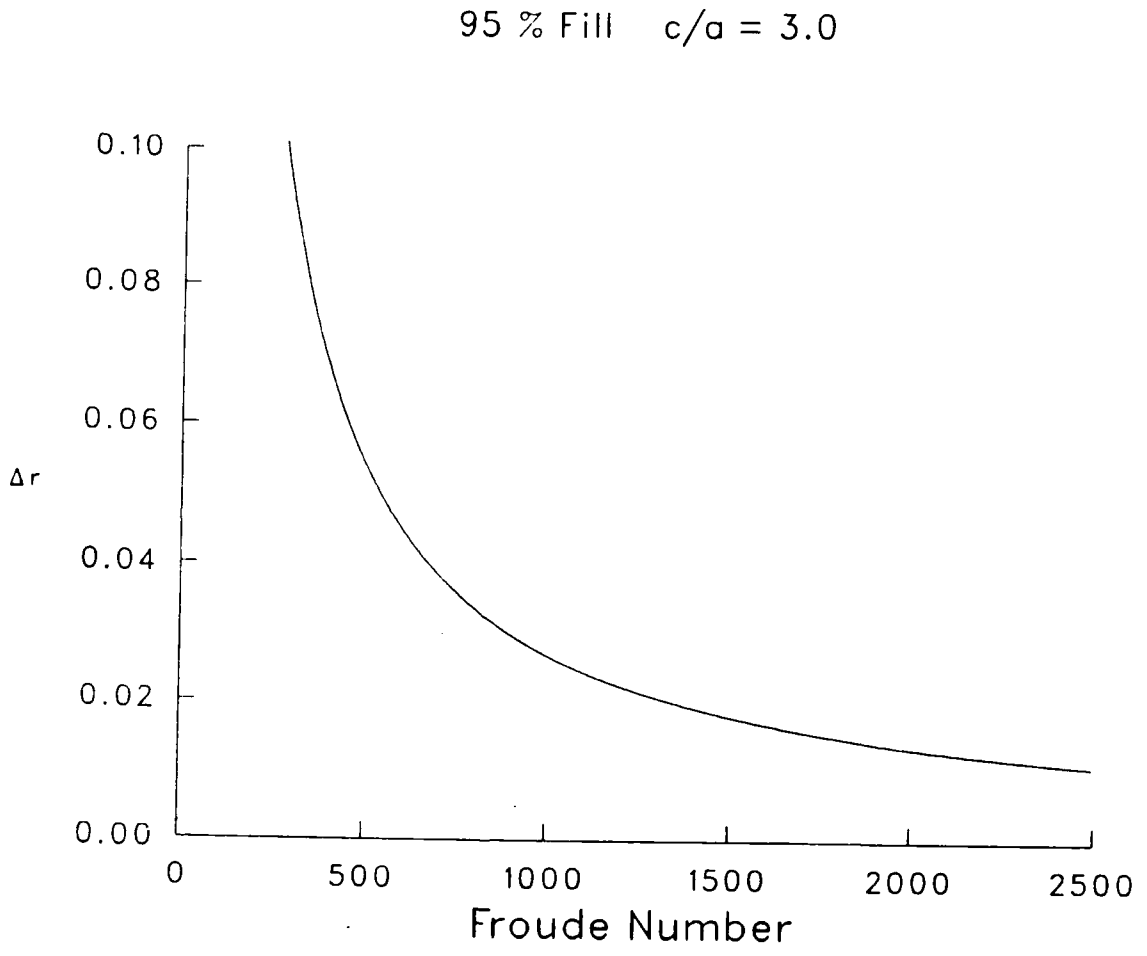

Figure 1. Difference in free surface radial location at the top wall and bottom wall of the cylinder as a function of Froude number, 95% fill

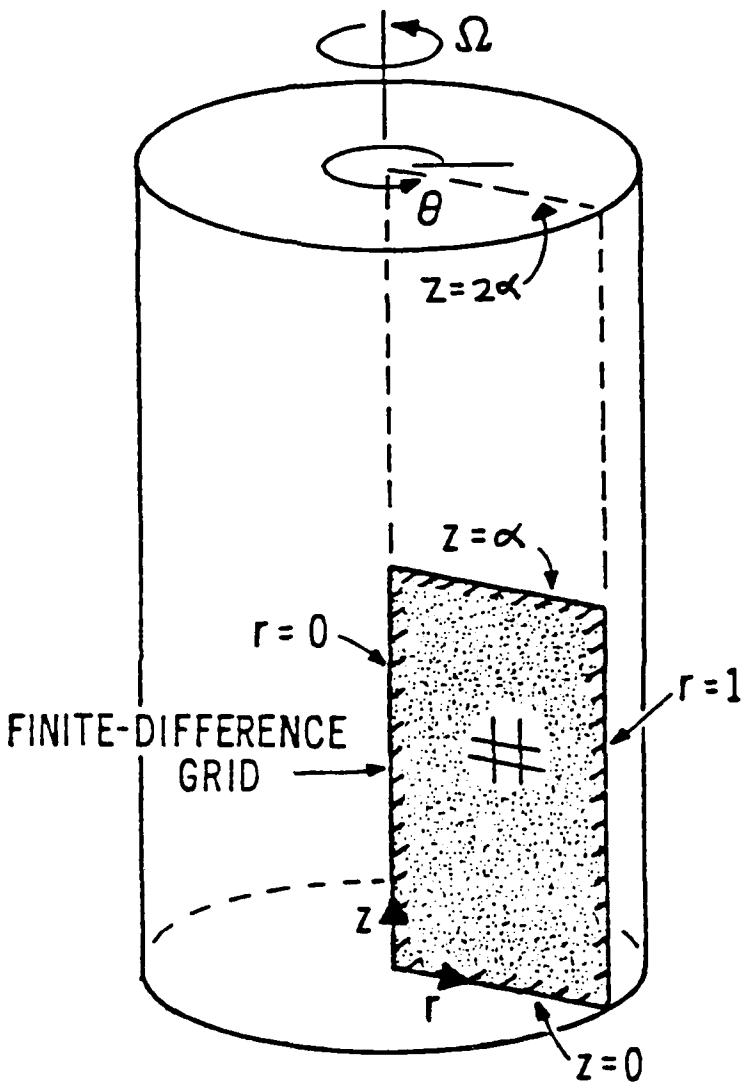

Figure 2. Cylinder geometry and computational domain

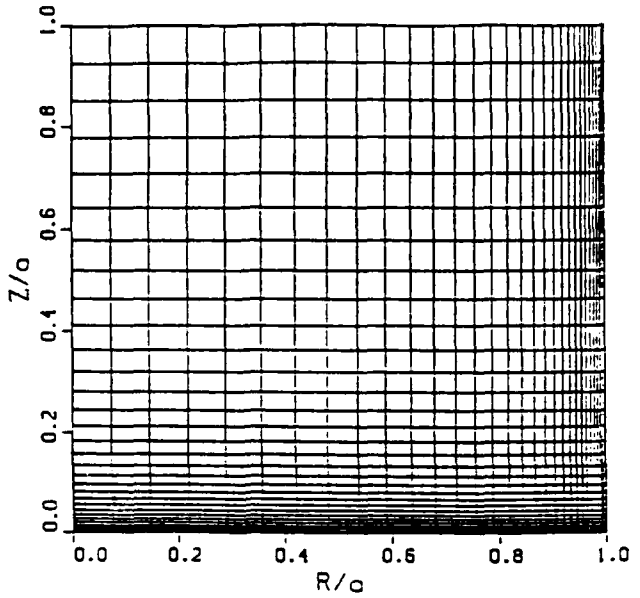

Figure 3. Finite-difference grid (31 x 31) with logarithmic stretching ($d = b = 0.05$) for full cylinder ($c/a = 1.0$)

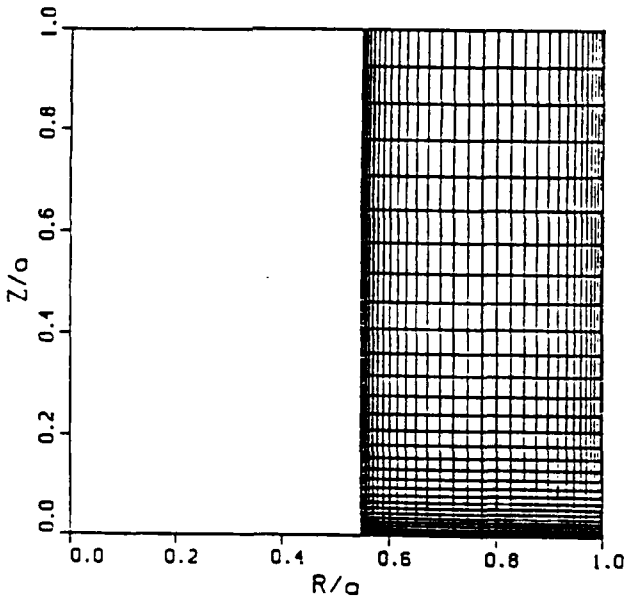

Figure 4. Finite-difference grid (31 x 31) with logarithmic stretching ($d = b = 0.05$) for 70% filled cylinder ($c/a = 1.0$)

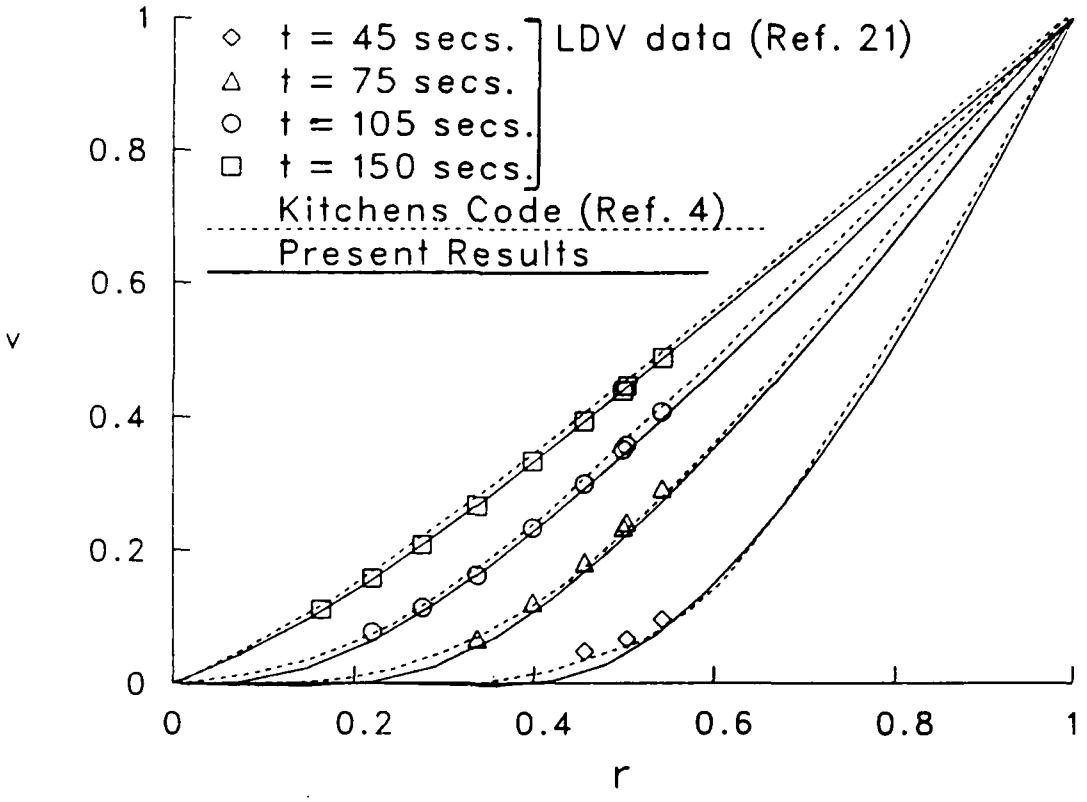

Figure 5. Azimuthal velocity profiles at cylinder midplane for $\alpha = 1$, Re = 9741.6

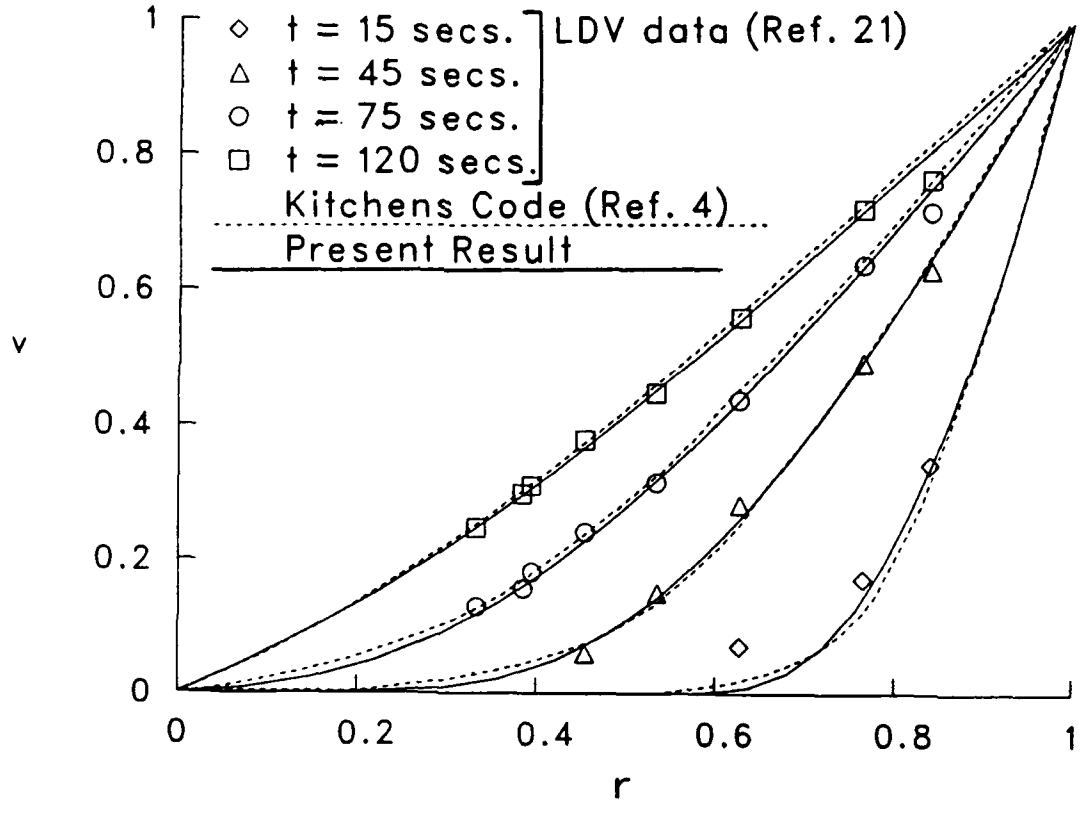

Figure 6. Azimuthal velocity profiles at cylinder midplane for $\alpha = 1.515$, Re = 3076

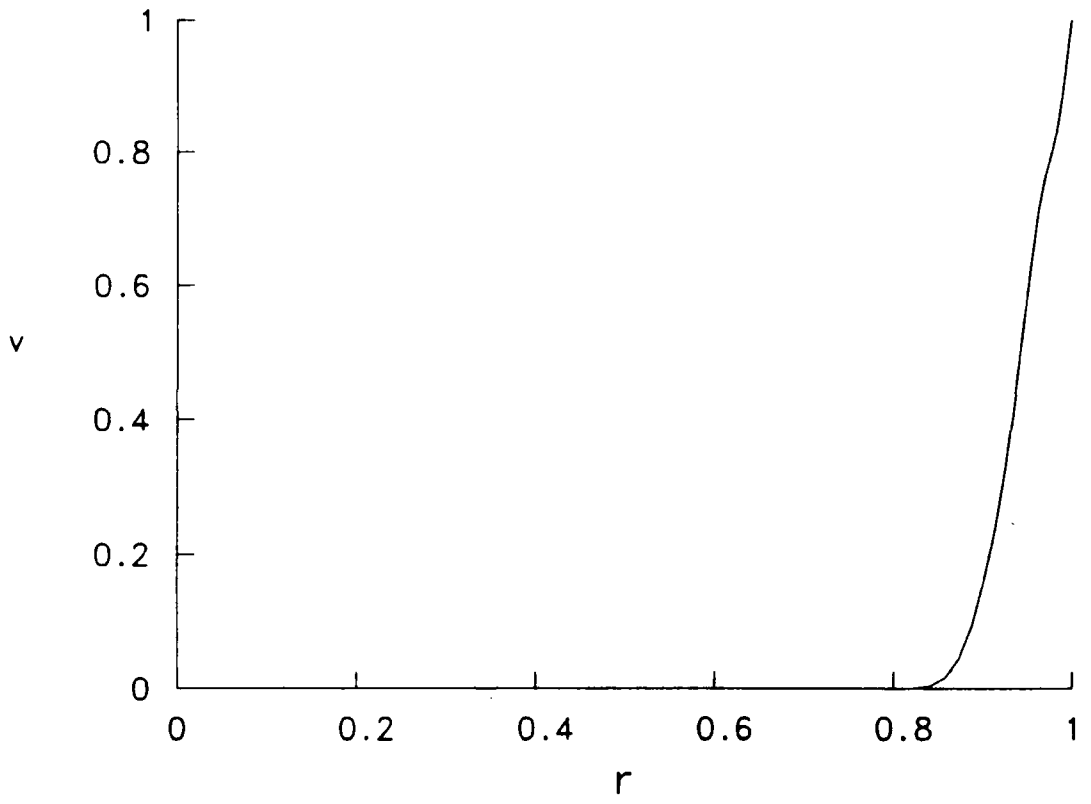

Figure 7. Azimuthal velocity profile near cylinder endwall ($z = 0.092$) for $\alpha = 1$, Re = 9741.6

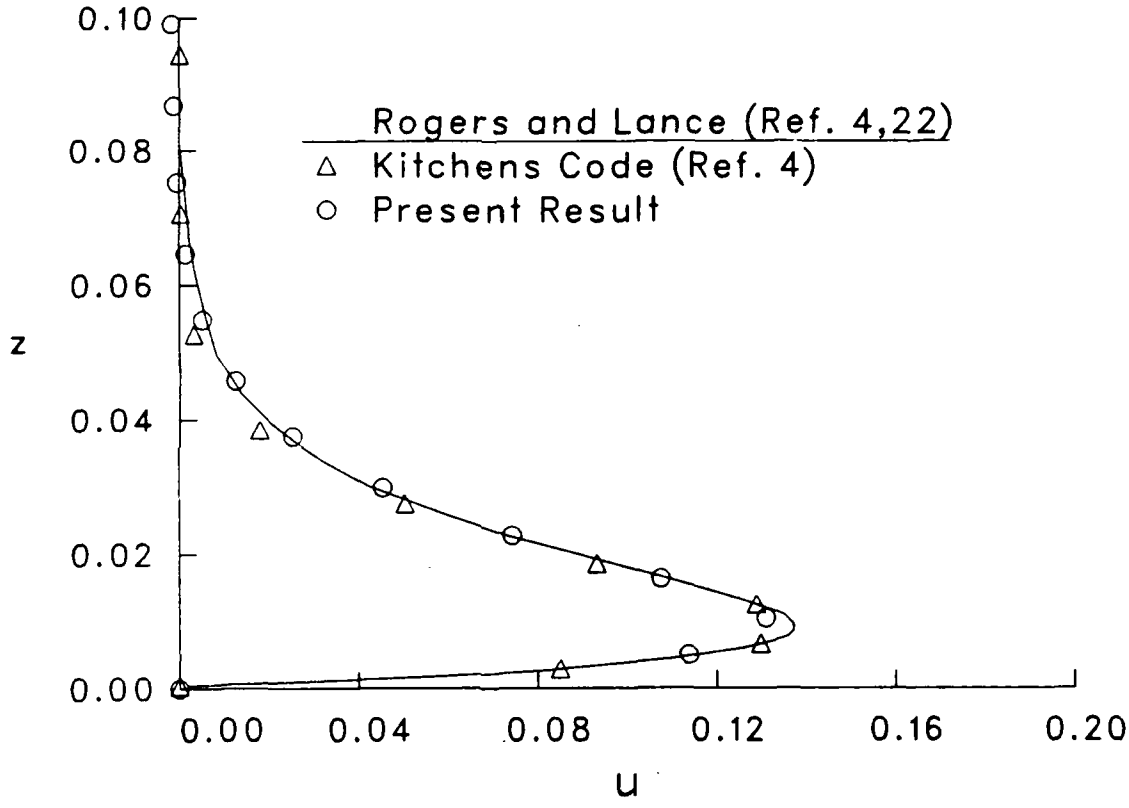

Figure 8. Radial velocity profile in Ekman layer at $r = 0.76$ for $\alpha = 1$, Re = 9741.6 and $t = 4.5$ sec.

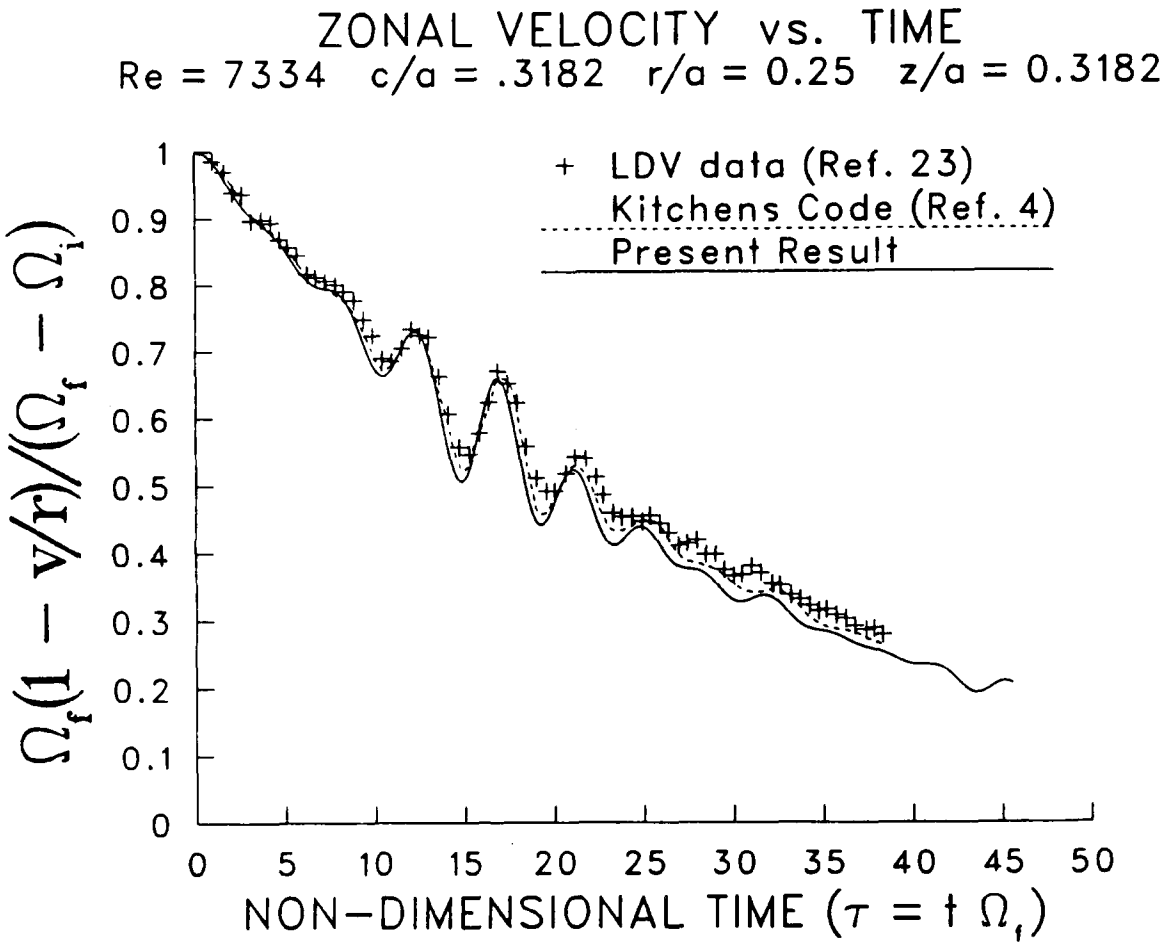

Figure 9. Inertial oscillations during spin-up from a previous state of rigid body rotation at $r = 0.25$, $z = 0.3182$

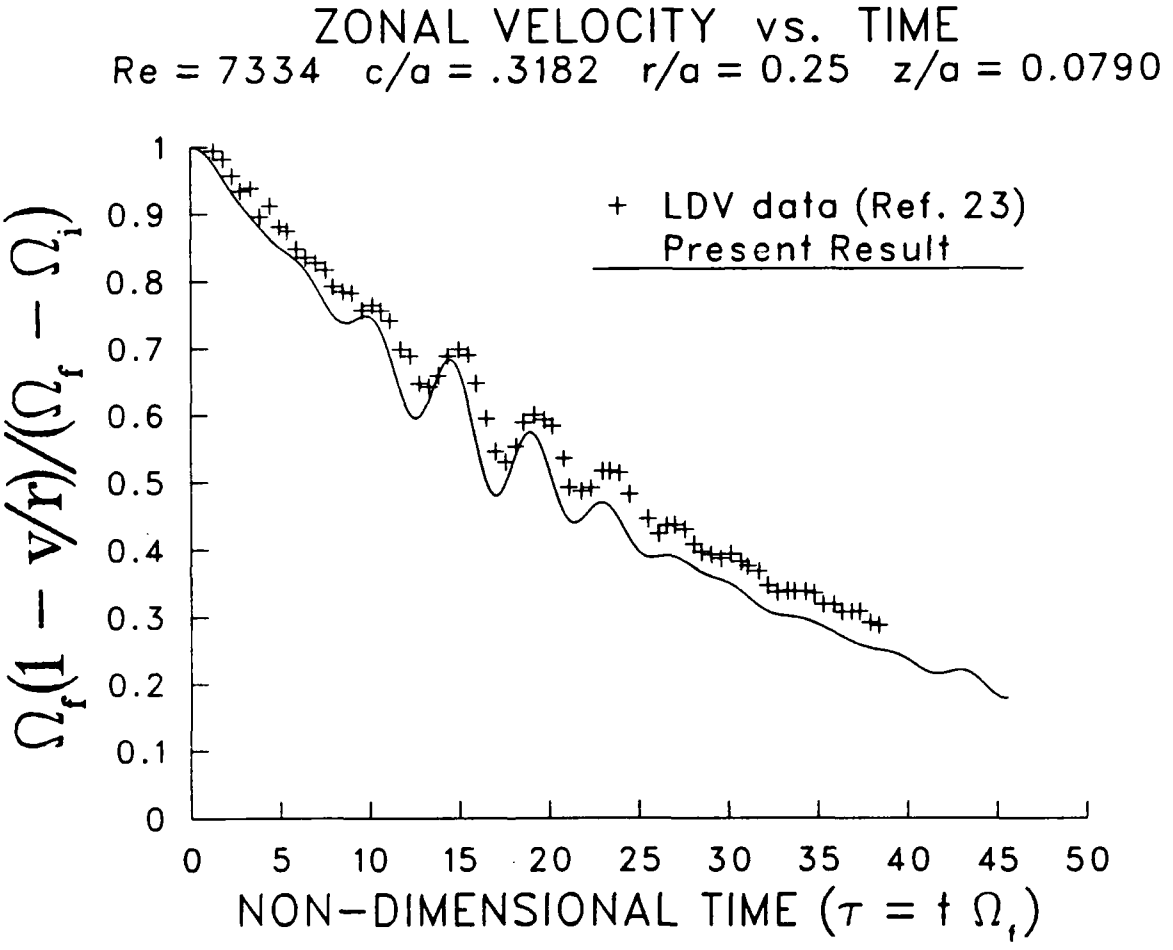

Figure 10. Inertial oscillations during spin-up from a previous state of rigid body rotation at $r = 0.25$, $z = 0.0790$

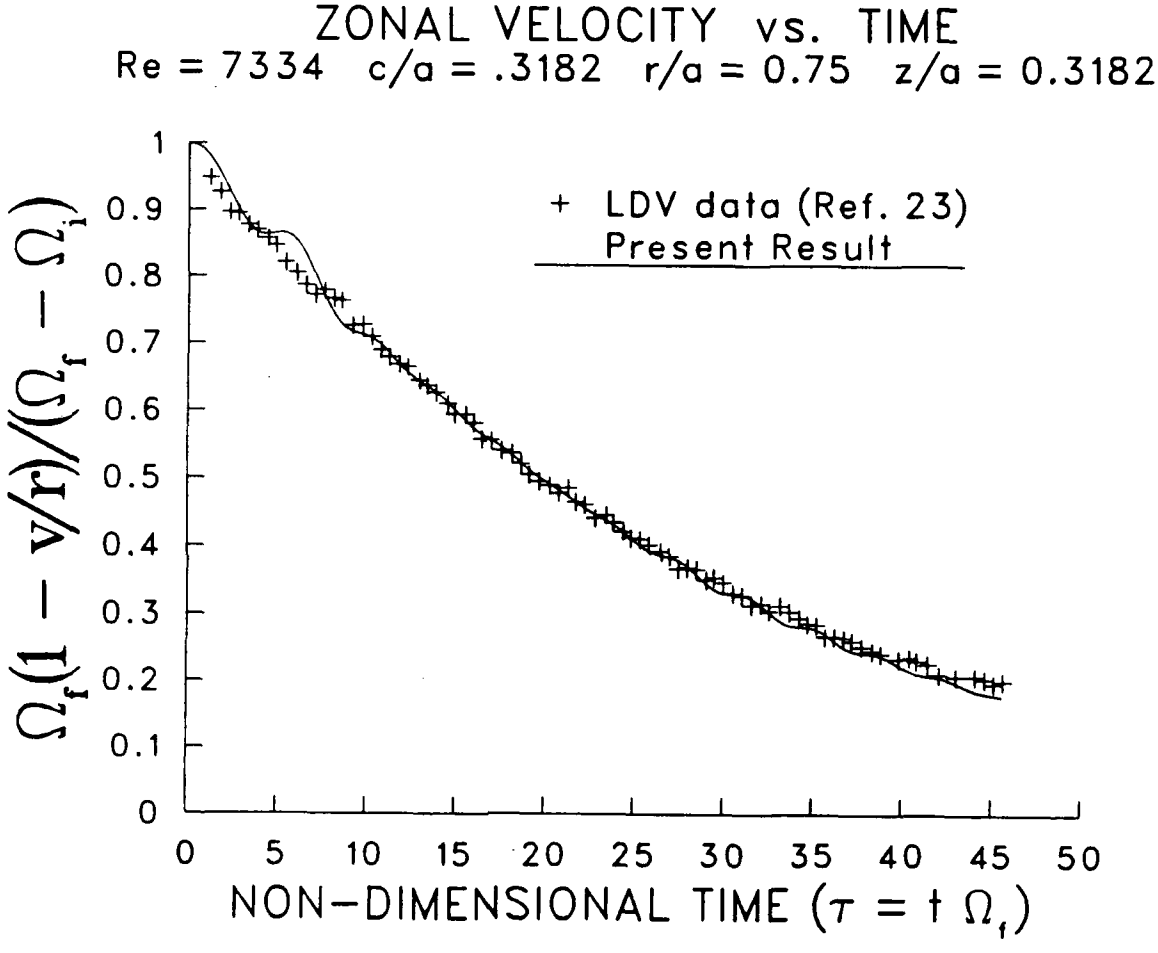

Figure 11. Inertial oscillations during spin-up from a previous state of rigid body rotation at $r = 0.75$, $z = 0.3182$

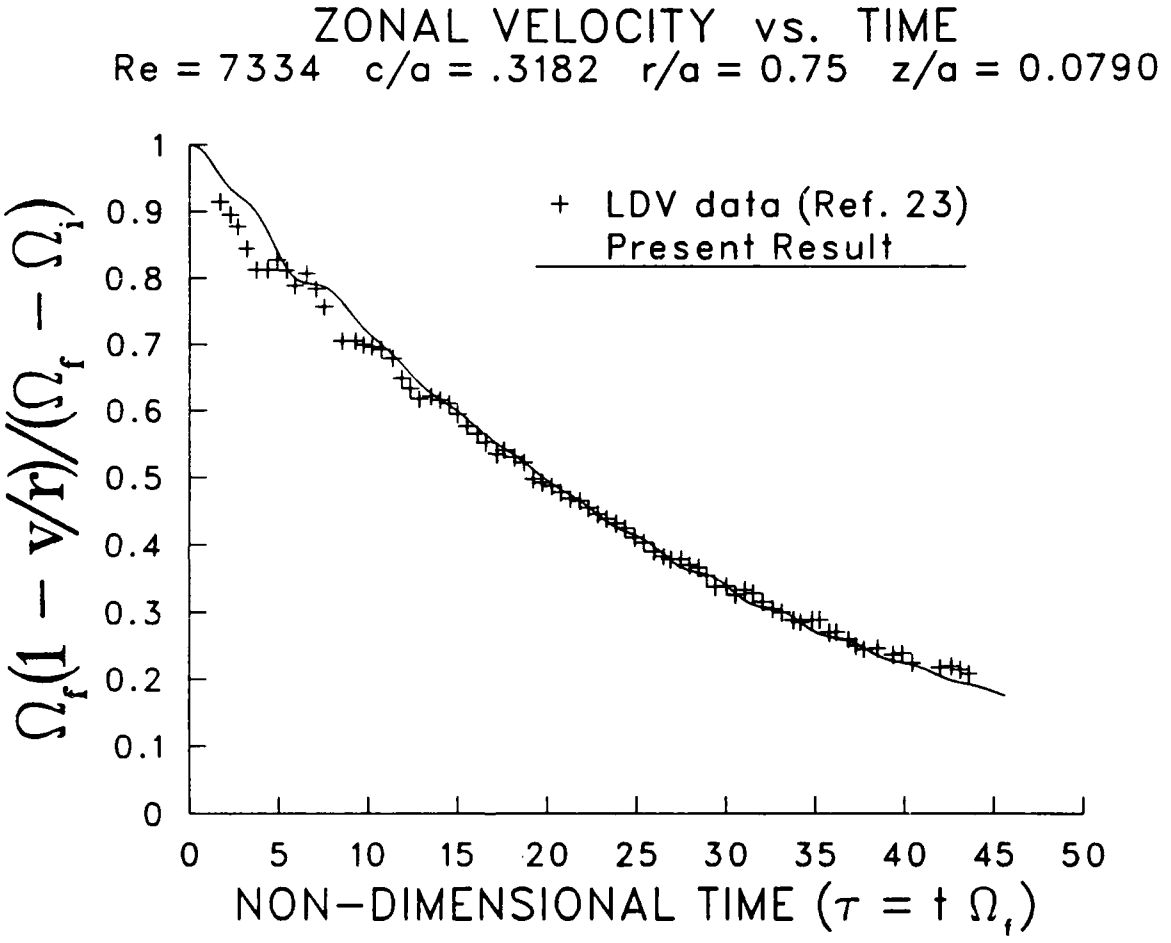

Figure 12. Inertial oscillations during spin-up from a previous state of rigid body rotation at $r = 0.75$, $z = 0.0790$

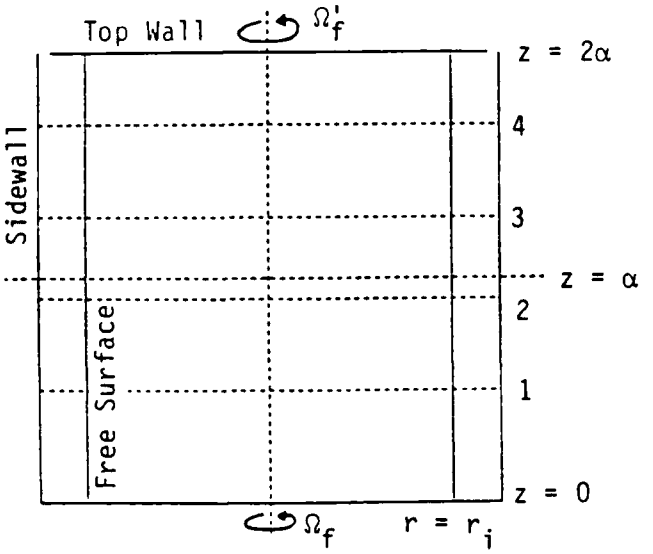

Figure 13. LDV measurement stations for liquid centrifuge experiment (Ref. 9); 1: $z = 0.497$, 2: $z = 0.9$, 3: $z = 1.304$, 4: $z = 1.706$

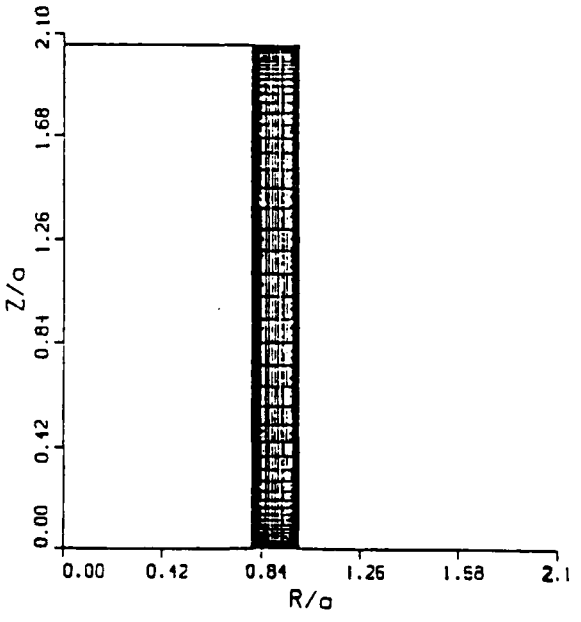

Figure 14. Finite-difference grid (30 x 61) for Re = 93518, $\alpha = 1.028$, 36.7% filled, $(\Delta z)_{endwalls} = 0.0018$, $(\Delta r)_{sidewall} = (\Delta r)_{free\ surface} = 0.0014$

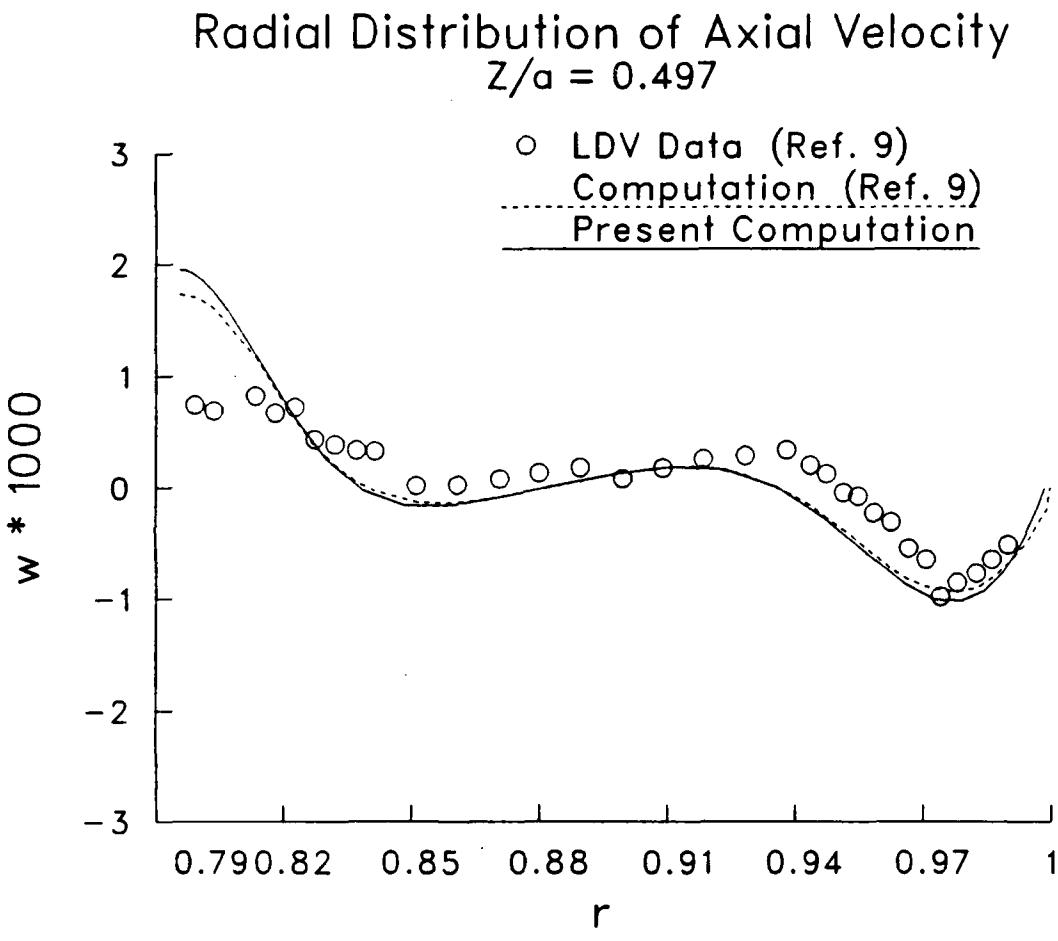

Figure 15. Axial velocity profile for Re = 93518, $\alpha = 1.028$, 36.7% filled, $z = 0.497$

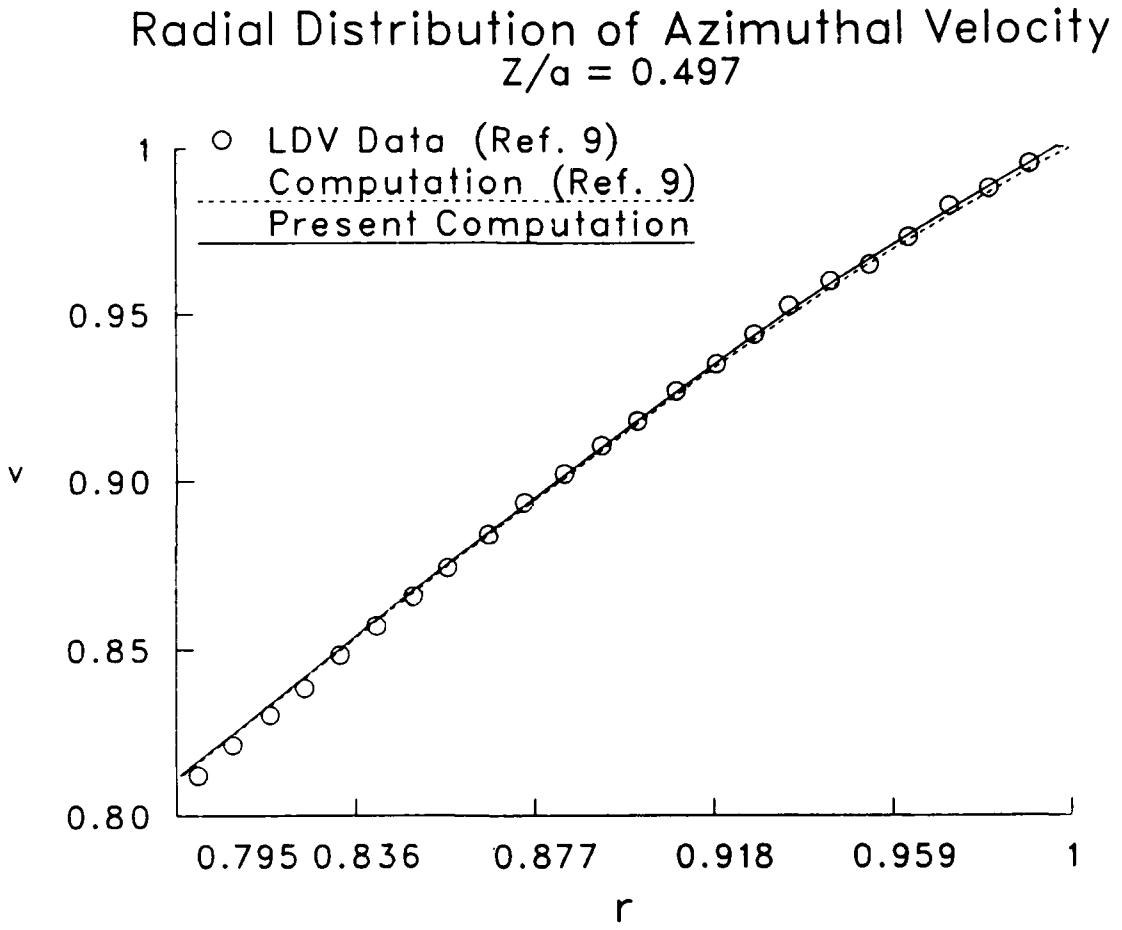

Figure 16. Azimuthal velocity profile for Re = 93518, $\alpha = 1.028$, 36.7% filled, $z = 0.497$

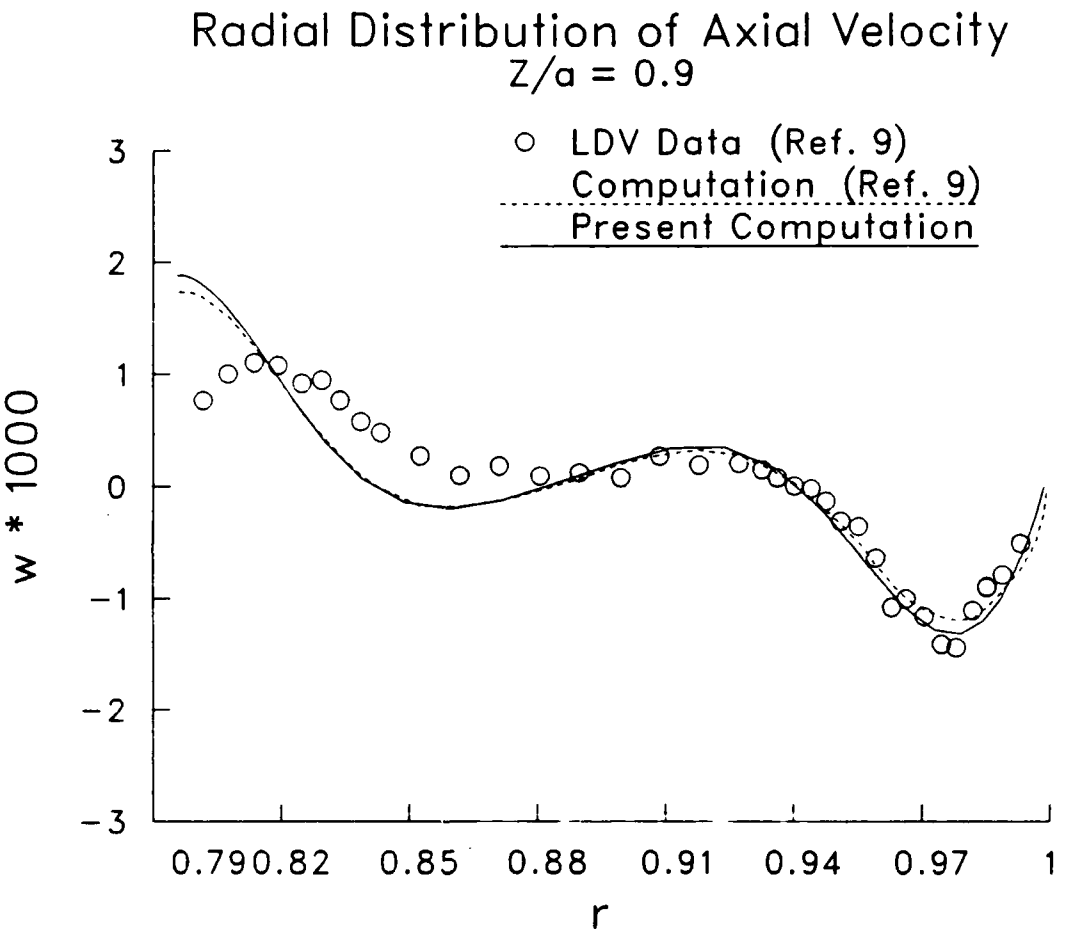

Figure 17. Axial velocity profile for Re = 93518, $\alpha = 1.028$, 36.7% filled, $z = 0.9$

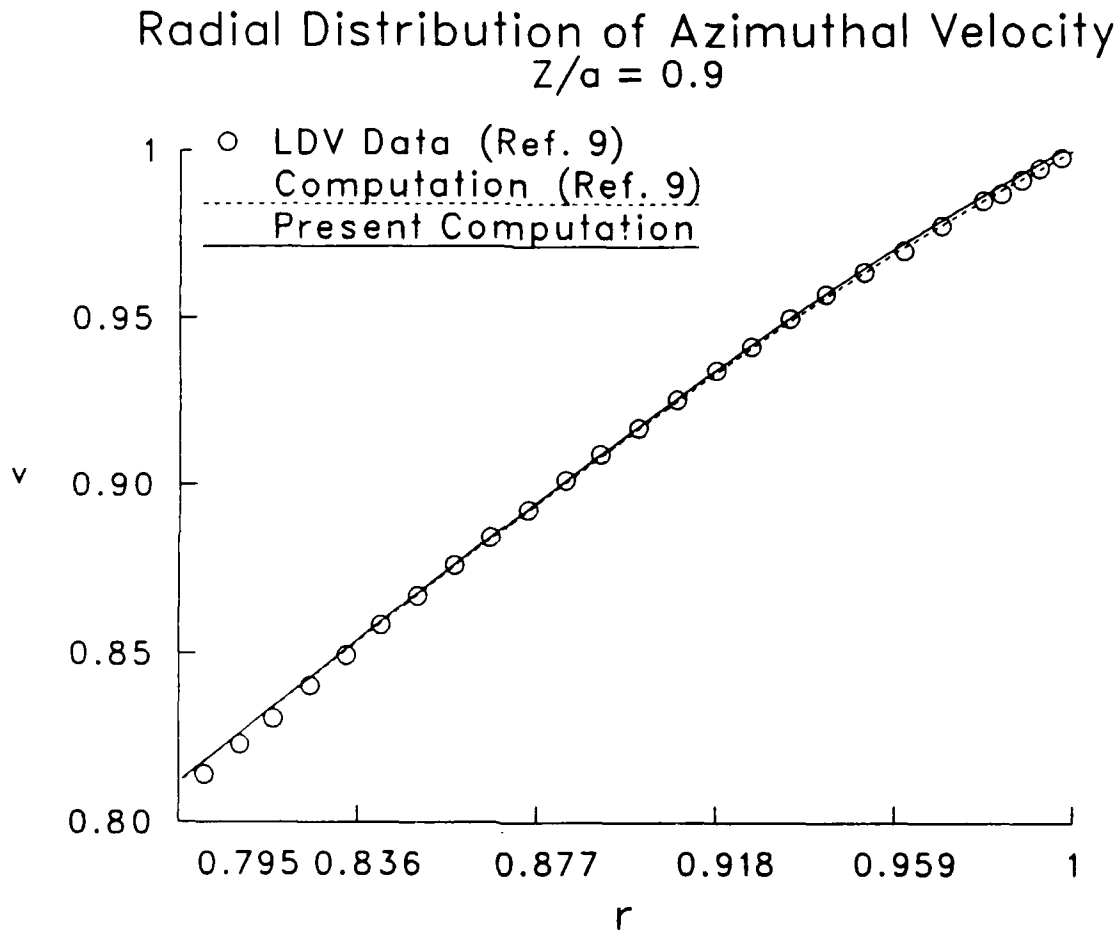

Figure 18. Azimuthal velocity profile for Re = 93518, $\alpha = 1.028$, 36.7% filled, $z = 0.9$

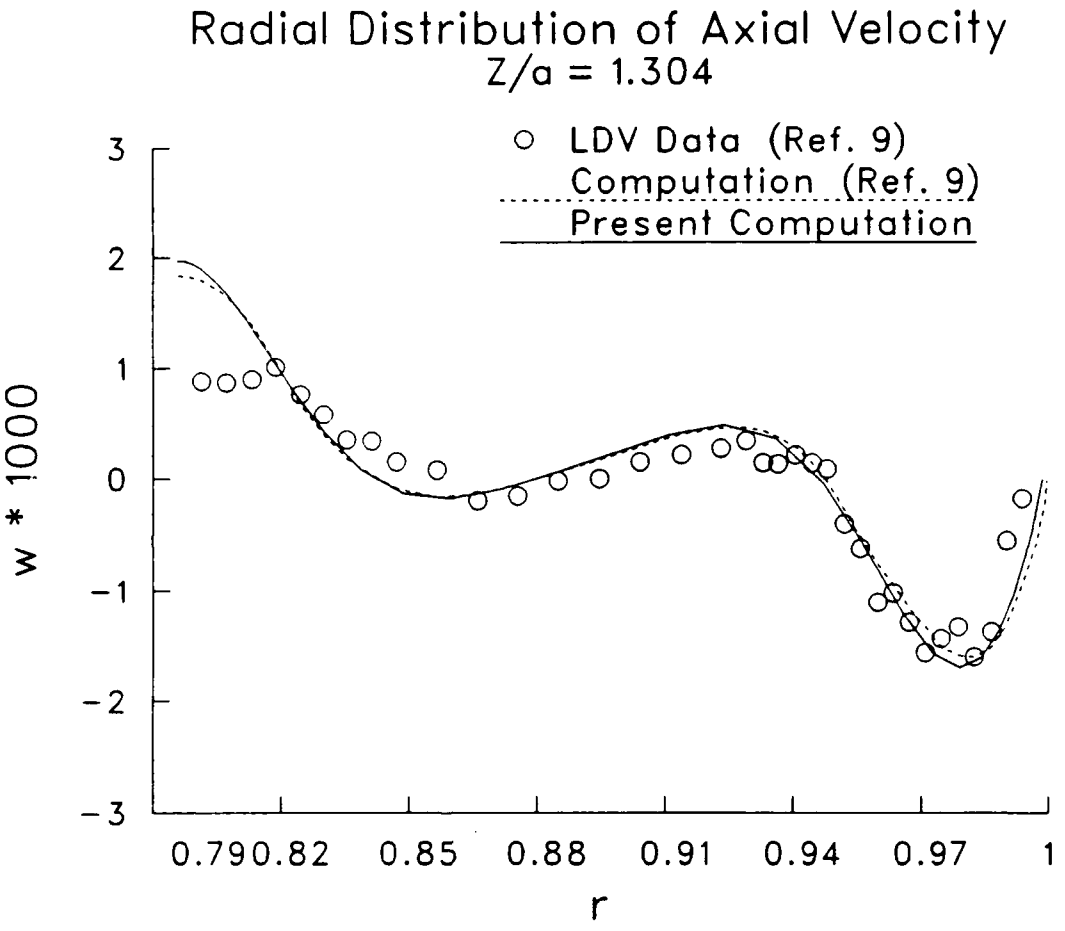

Figure 19. Axial velocity profile for Re = 93518, $\alpha = 1.028$, 36.7% filled, $z = 1.304$

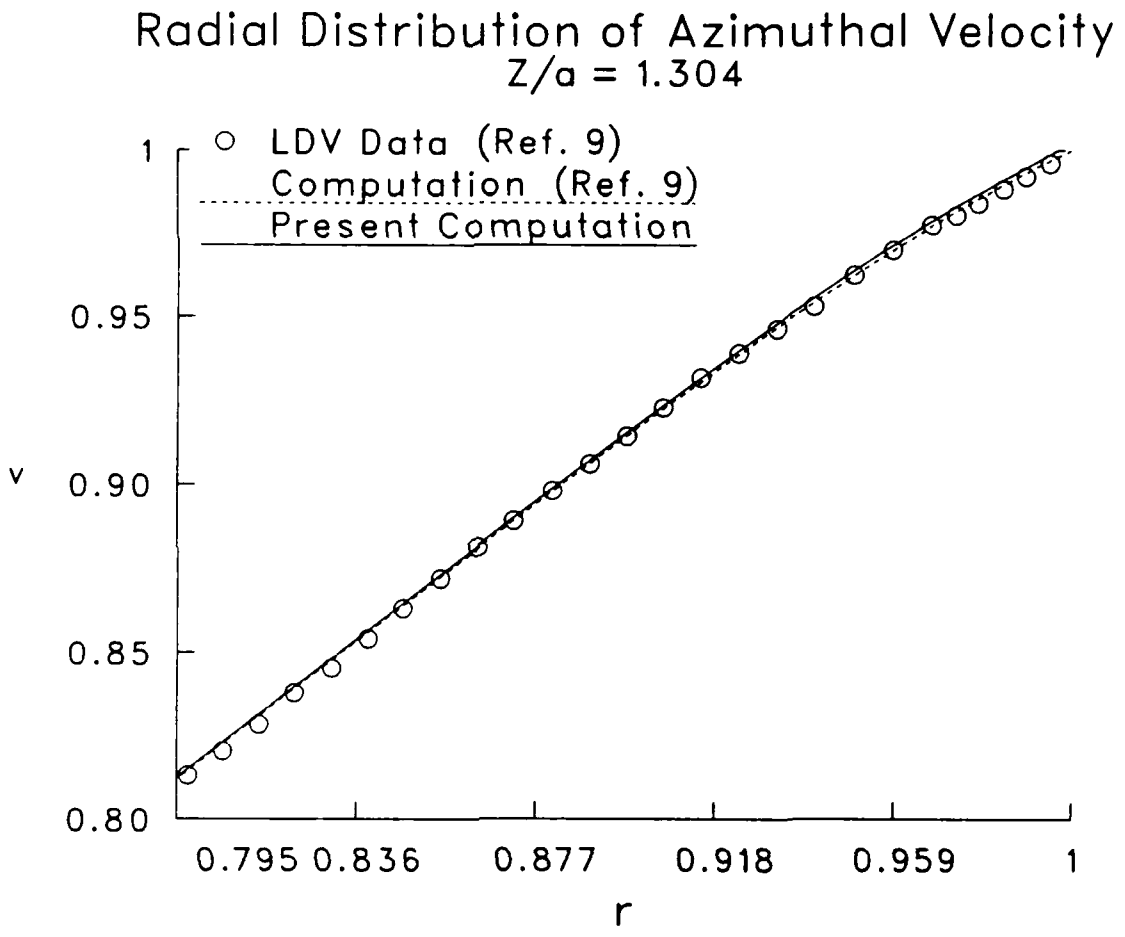

Figure 20. Azimuthal velocity profile for Re = 93518, $\alpha = 1.028$, 36.7% filled, $z = 1.304$

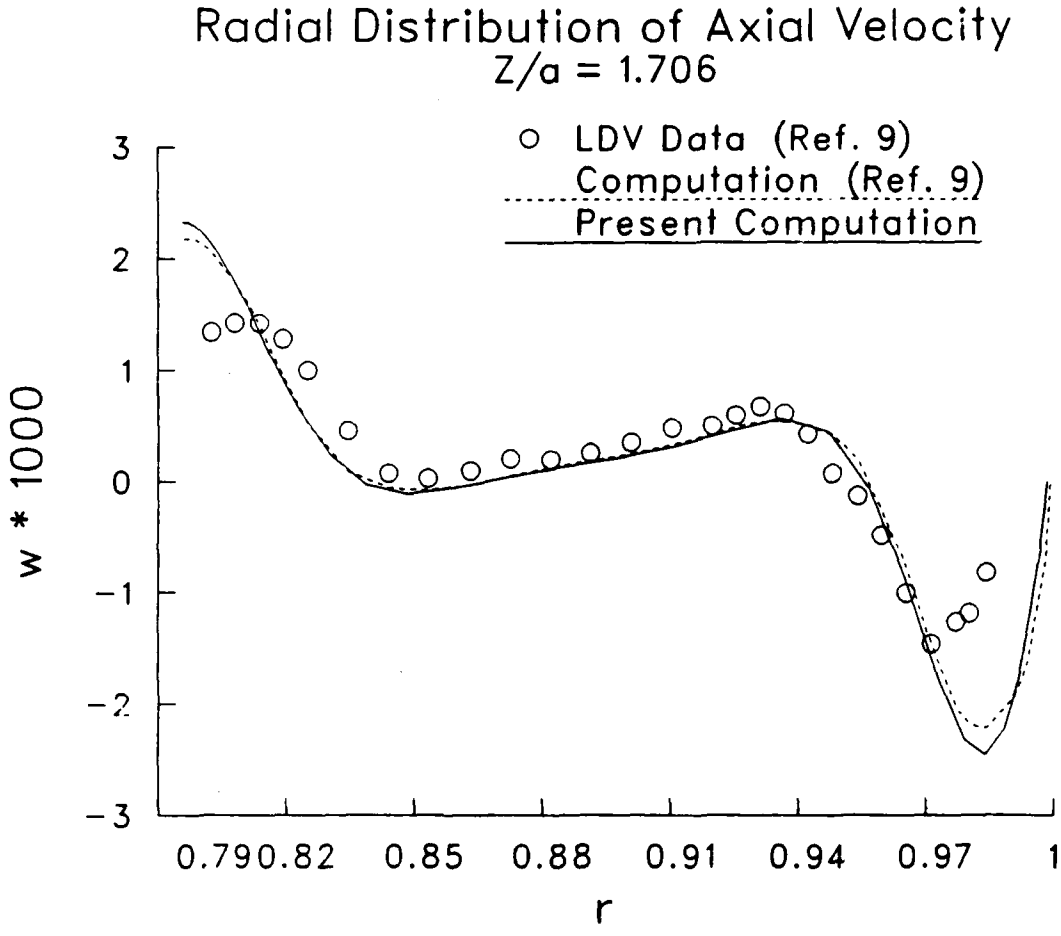

Figure 21. Axial velocity profile for Re = 93518, $\alpha = 1.028$, 36.7% filled, $z = 1.706$

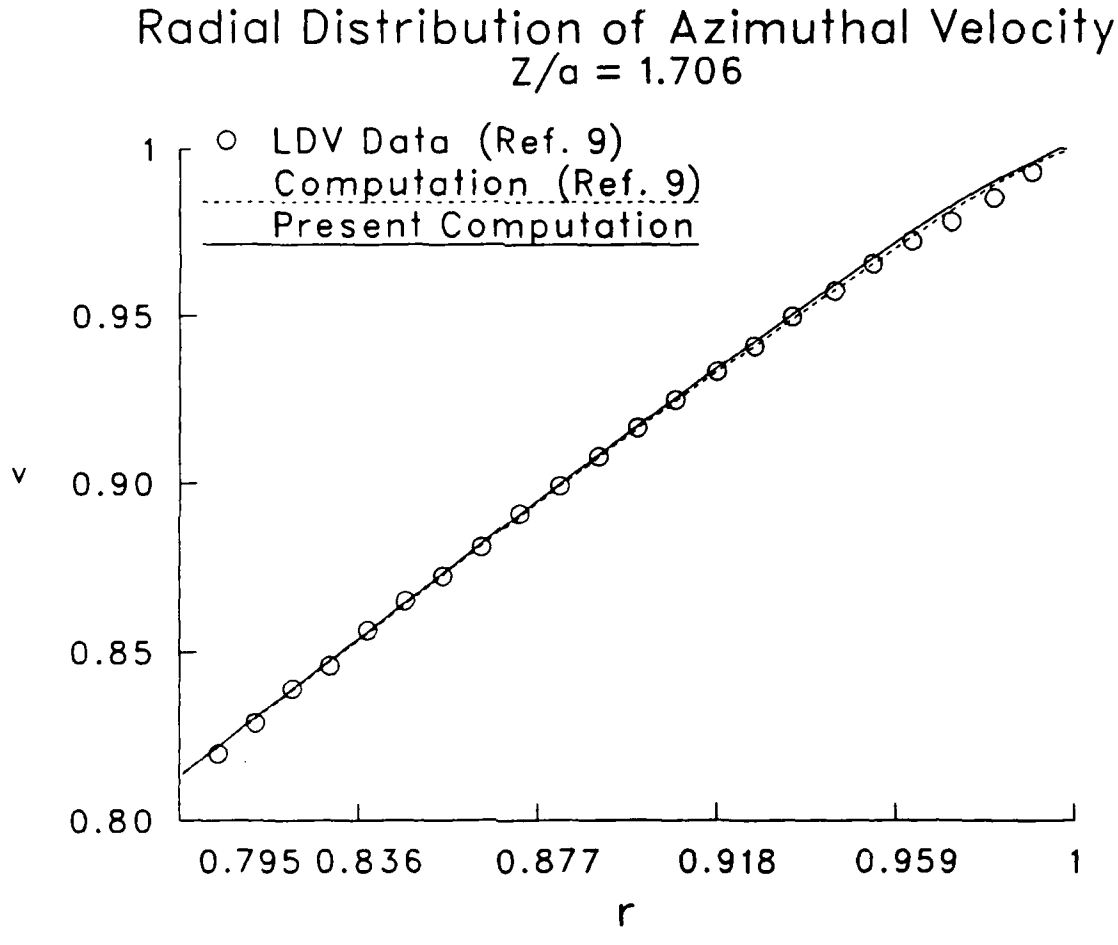

Figure 22. Azimuthal velocity profile for Re = 93518, $\alpha = 1.028$, 36.7% filled, $z = 1.706$

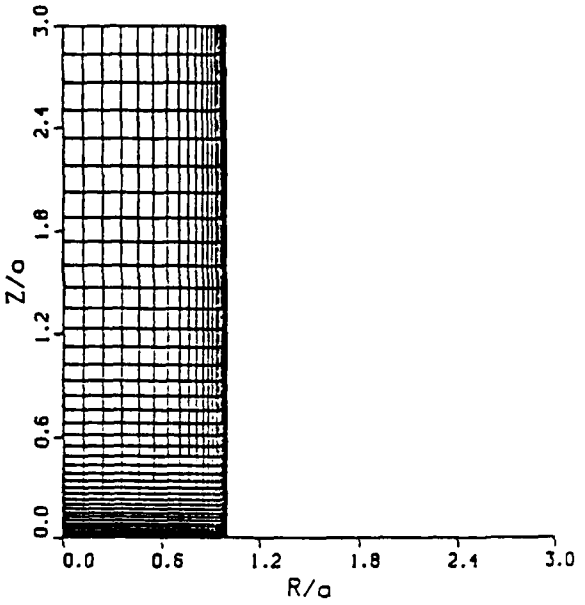

Figure 23. Finite-difference grid (21 x 41) for Re = 1000, $\alpha = 3$, full cylinder

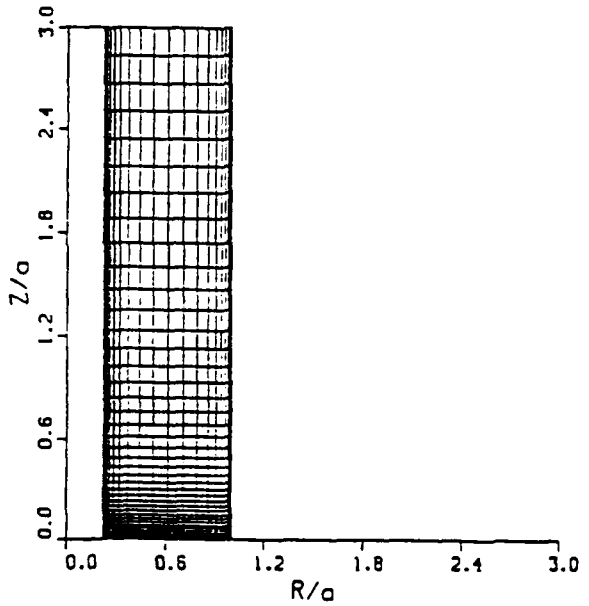

Figure 24. Finite-difference grid (21 x 41) for Re = 1000, $\alpha = 3$, 95% filled cylinder

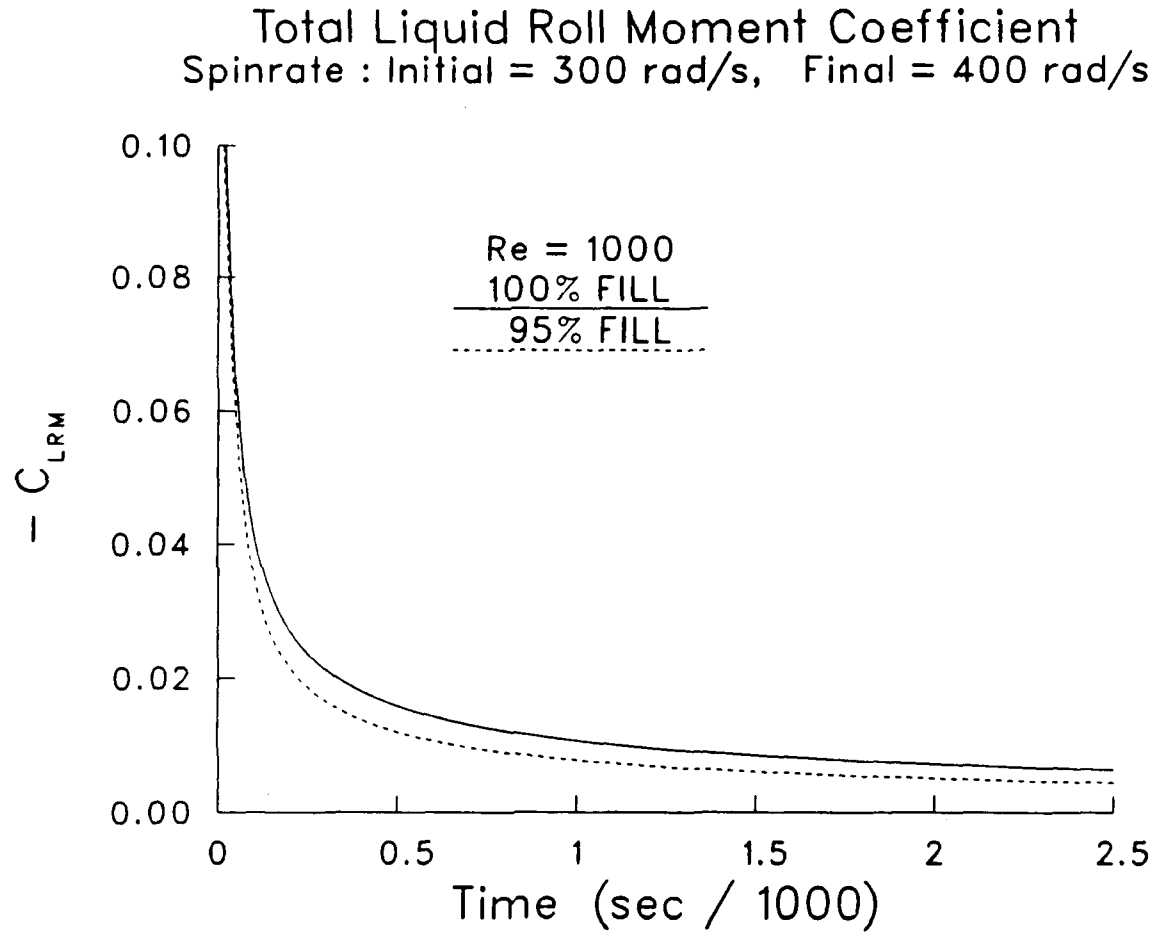

Figure 25. Total liquid roll moment coefficient vs time for Re = 1000, $\alpha = 3$, 100% and 95% filled cylinders

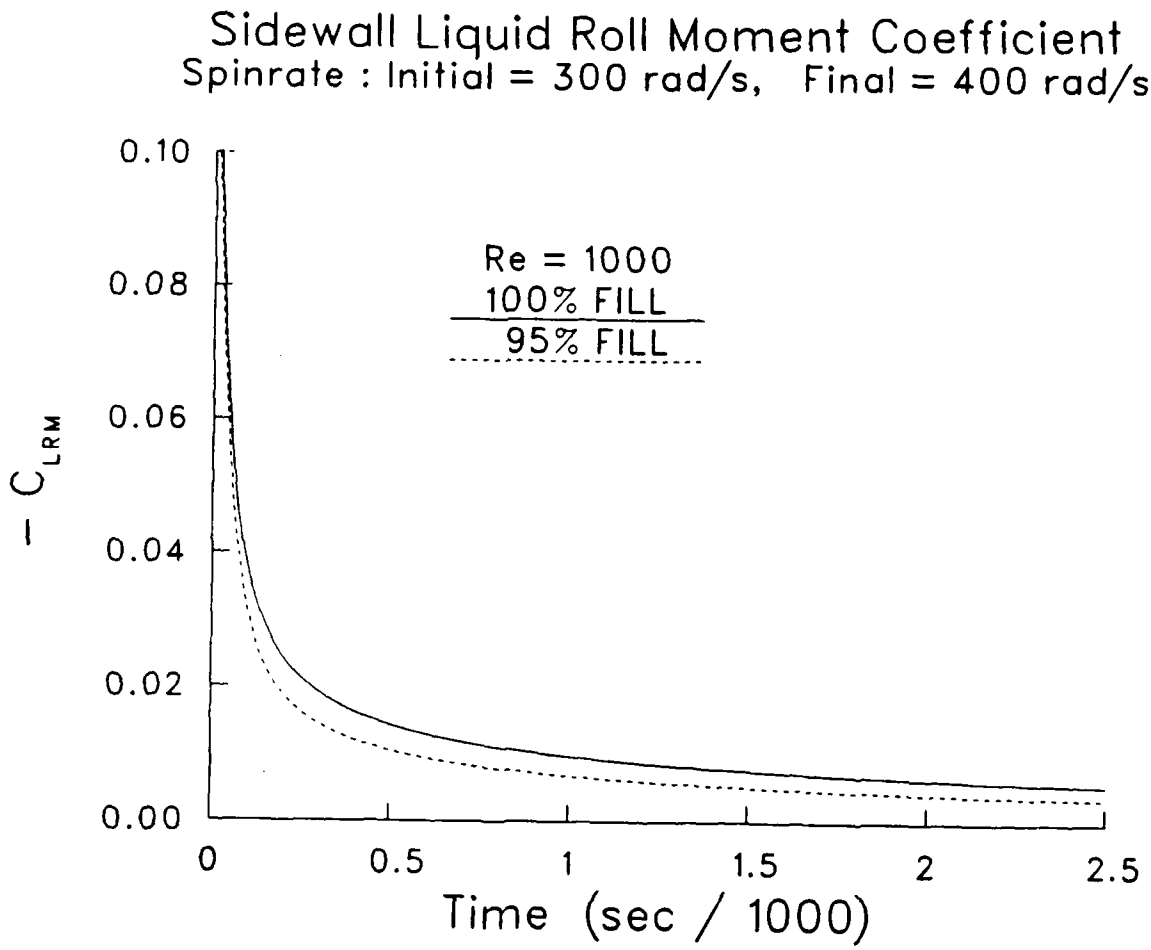

Figure 26. Sidewall component of liquid roll moment coefficient vs time for Re = 1000, $\alpha = 3$, 100% and 95% filled cylinders

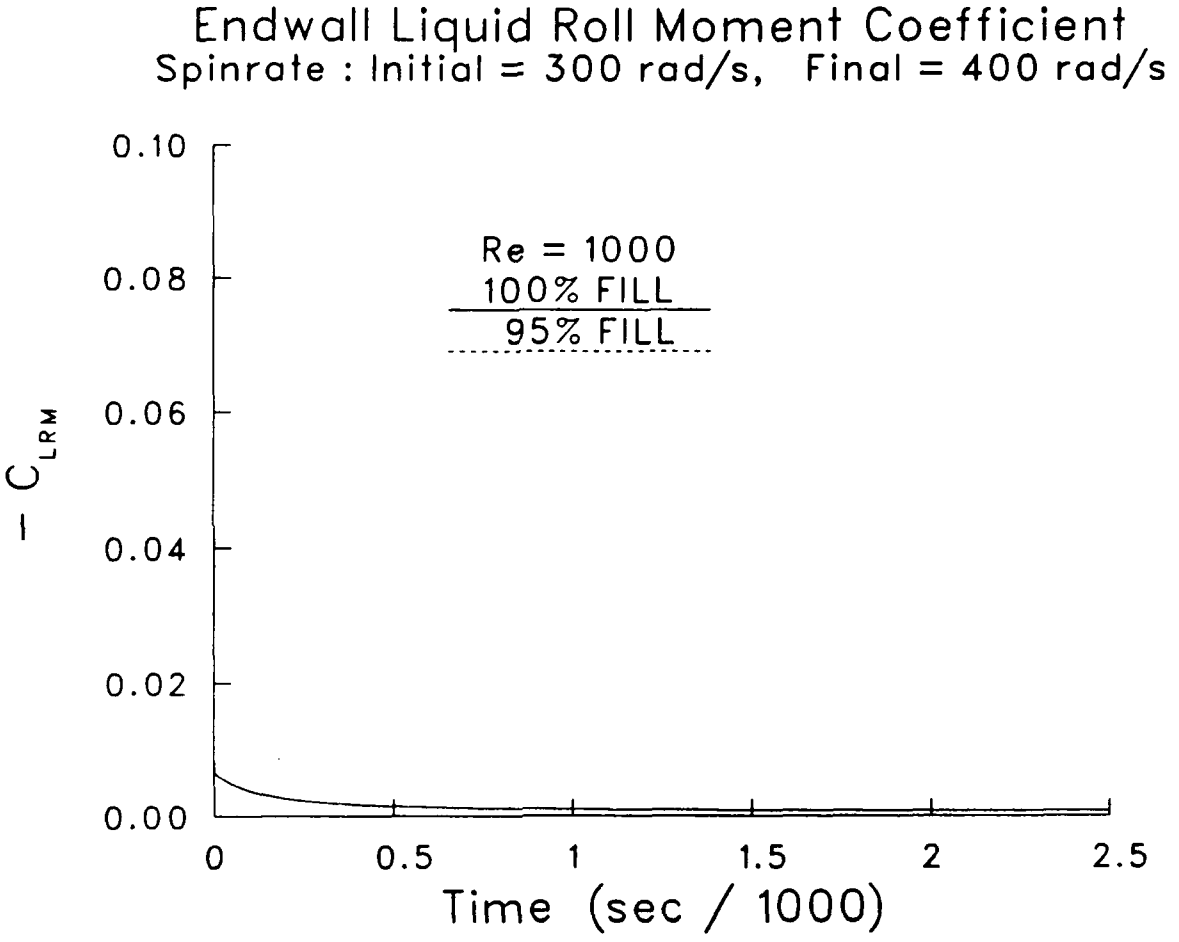

Figure 27. Endwall component of liquid roll moment coefficient vs time for Re = 1000, $\alpha = 3$, 100% and 95% filled cylinders

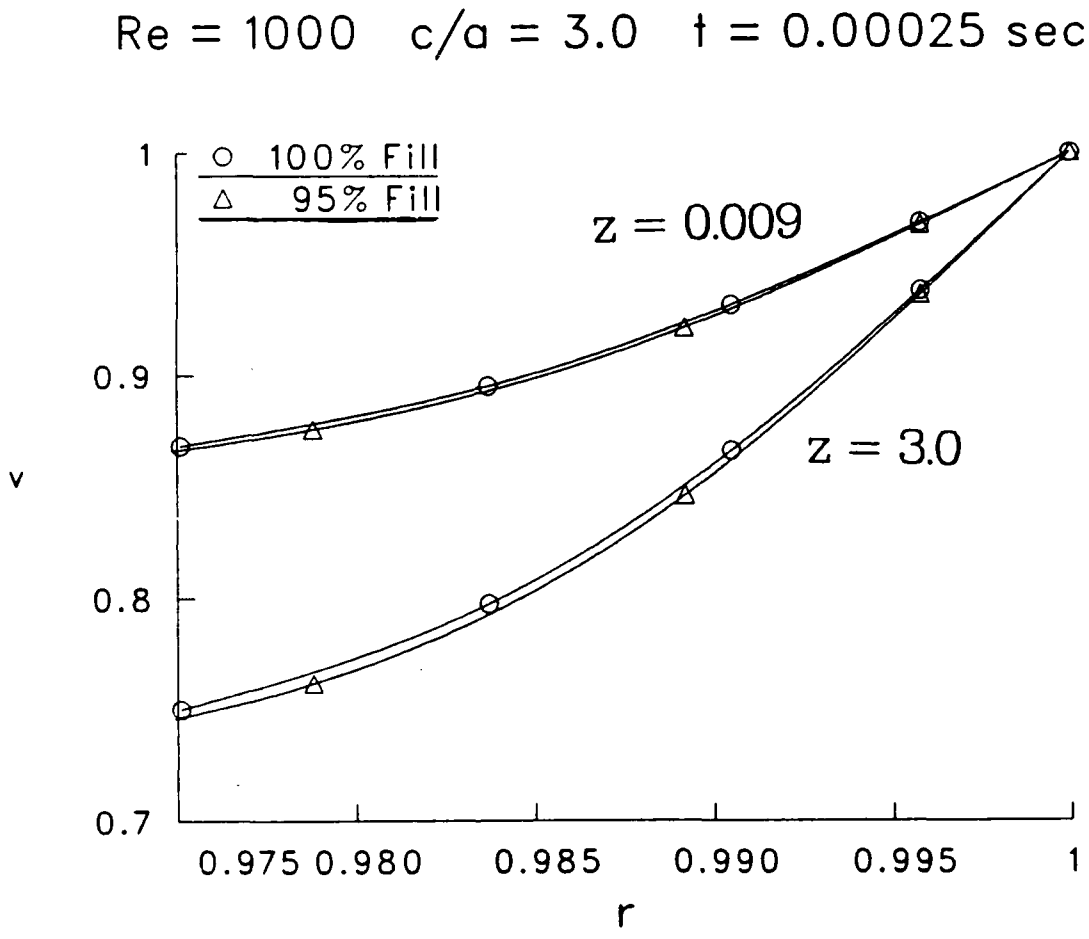

Figure 28. Azimuthal velocity profiles for $z = 0.009$ and 3.0 for Re = 1000, $\alpha = 3$, $t =$ 0.00025 sec, 100% and 95% filled cylinders

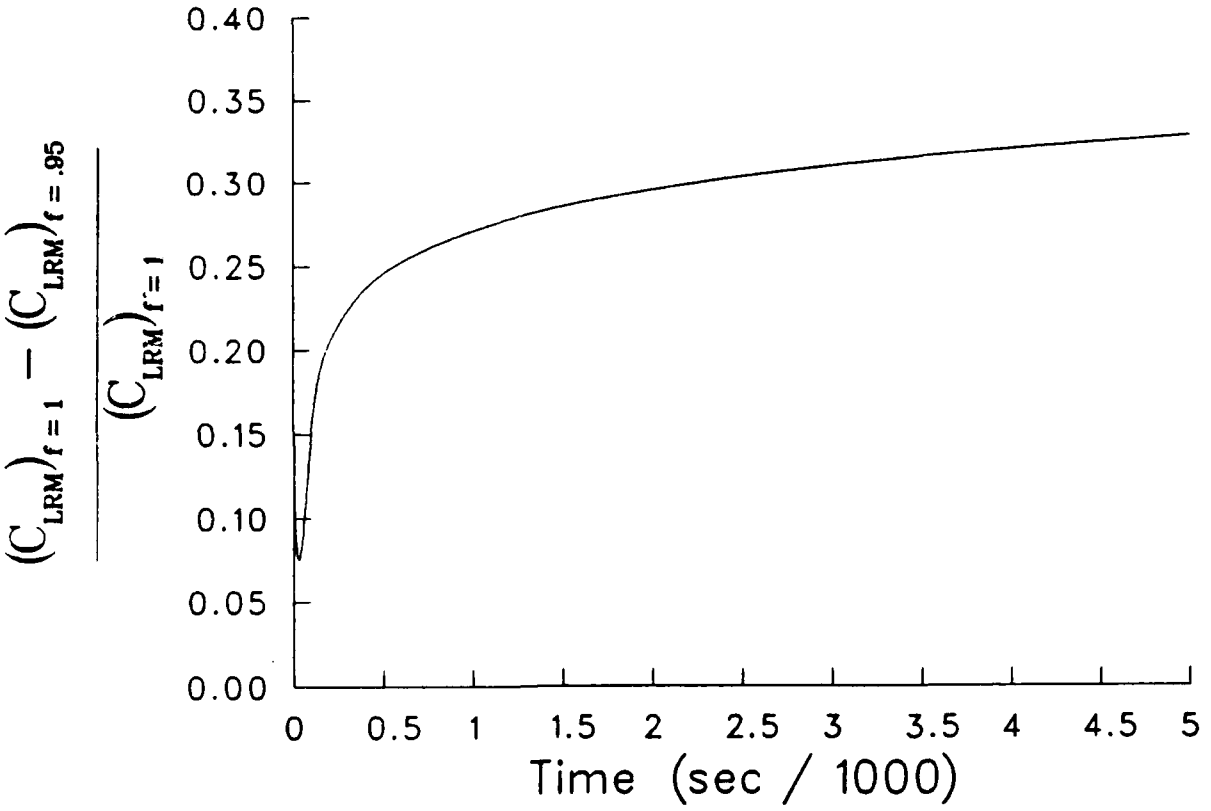

Figure 29. Relative difference in total liquid roll moment coefficient for $f = 1$ and $f = 0.95$ vs time for Re = 1000, $\alpha = 3$

References

1. Stewartson, K., "On the Stability of a Spinning Top Containing Liquid," Journal of Fluid Mechanics, Vol. 5, Part 4., pp.577-592, 1959.

2. Sedney, R., "A Survey of the Fluid Dynamic Aspects of Liquid-Filled Projectiles," Proceedings of the 12th AIAA Atmospheric Flight Mechanics Conference, August 19-21, 1985, Snowmass, Colorado.

3. Miller, M. C., "Void Characteristics of a Liquid-Filled Cylinder Undergoing Spinning and Coning Motion," Journal of Spacecraft and Rockets, Vol. 18, No. 3, May-June 1981, pp. 286-288.

4. Kitchens, Clarence W., "Navier-Stokes Solutions for Spin-up in a Filled Cylinder," ARBRL-TR-02193, U.S. Army Ballistic Research Laboratory, Aberdeen Proving Ground, Maryland, September 1979. (AD A077115) (See also AIAA Journal, Vol. 18, No. 8, pp 929-934, 1979.)

5. Rubin, S. G., and Lin T. C., "A Numerical Method for Three-Dimensional Viscous Flow: Application to the Hypersonic Leading Edge," Journal of Computational Physics, Vol. 9, 1972, pp. 339-364.

6. Chakravarthy, Sukumar R., "Numerical Simulation of Laminar, Incompressible Flow Within Liquid-Filled Shells," ARBRL-CR-00491, U.S. Army Ballistic Research Laboratory, Aberdeen Proving Ground, Maryland, November 1982. (AD A121703)

7. Homicz, Gregory F., and Gerber, Nathan, "Numerical Model for Fluid Spin-up From Rest in a Partially-Filled Cylinder," AIAA-86-1121, Proceedings of the 14th AIAA/ASME Joint Fluid Mechanics, Plasmadynamics and Lasers Conference Atlanta, Ga., 1986.

8. Goller, H. and Ranov, T., "Unsteady Rotating Flow in a Cylinder With a Free Surface," Transaction of the ASME, Journal of Basic Engineering, December 1968, pp. 445-454.

9. Shadday, Martin A., Jr., "Flow in a Partially-Filled Rotating Cylinder," Ph.D. Dissertation, University of Virginia, May 1982. (See also Journal of Fluid Mechanics, Vol. 130, pp.203-218, 1983).

10. Chorin, A. J., "A Numerical Method for Solving Incommpressible Viscous Flow Problems," Journal of Computational Physics, Vol. 2, pp.12-26, 1967.

11. Winch, David M., "An Investigation of the Liquid Level at the Wall of a Spinning Tank," NASA TND-1536, NASA Lewis Research Center, August 1962.

12. Gerber, Nathan, "Rigidly Rotating Liquids in Closed Partially-Filled Cylindrical Cavities," ARBRL-MR-02462, U.S. Army Ballistic Research Laboratory, Aberdeen Proving Ground, Maryland, March 1975. (AD A008318)

13. Nusca, Michael J., "Numerical Investigation of Unsteady Viscous Incompressible Liquid Flow in a Partially-Filled Rotating Cylinder," M.S. Thesis, Dept. of Aerospace Engineering, University of Maryland, College Park, Md., 1986.

14. Harlow, F. H. and Welch, J. E., "Numerical Calculation of Time-Dependent Viscous Incompressible Flow of Fluid with Free Surface," The Physics of Fluids, Vol. 8, No. 12, December 1965, pp. 2182-2189.

15. Steger, Joseph L. and Chakravarthy, Sukumar R., "Computational Fluid Dynamics of Liquid-Filled Spinning Shells," U.S. Army Ballistic Research Laboratory, Aberdeen Proving Ground, Maryland, Contract Report in preparation.

16. Roache, Patrick J., "Computational Fluid Dynamics," Hermosa Publishers, Albuquerque, New Mexico, 1982.

17. Anderson, D. A., Tannehill, J. C., Pletcher, R. H., "Computational Fluid Mechanics and Heat Transfer," Hemisphere Publishing Corporation, McGraw Hill, 1984.

18. Peyret, R., Taylor, T. D., "Computational Methods for Fluid Flow," Springer Series in Computational Physics, Springer-Verlag, 1983.

19. Roberts, Glyn O., "Computational Methods for Boundary Layer Problems," Lecture Notes in Physics, Vol. 8, Proceedings of the Second International Conference on Numerical Methods in Fluid Dynamics, September 15-19, 1970.

20. Carnahan, B., Luther, H. A., and Wilkes, J. O., "Applied Numerical Methods," John Wiley and Sons, New York, 1969.

21. Watkins, W. B., and Hussey, R. G., "Spin-Up From Rest in a Cylinder," The Physics of Fluids Vol. 20, No. 10, Pt. 1, October 1977, pp. 1596-1604.

22. Rogers, M. H., and Lance, G. N., "The Rotationally Symmetric Flow of a Viscous Fluid in the Presence of an Infinite Rotating Disk," Journal of Fluid Mechanics, Vol. 7, Pt. 4, April, 1960, pp. 617-631.

23. Warn-Varnas, A., Fowlis, W. W., Piacsek, S., and Lee, S. M., "Numerical Solutions and Laser-Doppler Measurements of Spin-Up," Journal of Fluid Mechanics, Vol. 85, Pt. 4, 1978, pp. 609-639.

24. Murphy, C. H., "A Relation Between Liquid Roll Moment and Liquid Side Moment," Journal of Guidance, Control and Dynamics, Vol. 8., No. 2, pp. 27-288, March-April 1985.

List of Symbols

a	cylinder radius
b	grid stretching parameter for the z-direction (see Eq. 35)
c	cylinder half-height
d	grid stretching parameter for the r-direction (see Eq. 34)
C_{LRM}	coefficient of liquid roll moment
E	Ekman number, $\nu/\Omega_f c^2$, the ratio of viscous to Coriolis force.
f	liquid fill ratio of the cylinder, $Z_i/(2c)$
Fr	Froude number, $\Omega_f^2 a/g$
g	gravitational acceleration, 9.81 ft/sec^2
P, p	dimensional, nondimensional local pressure, inertial reference frame, $p = P/\rho\Omega_f^2 a^2$
R, r	dimensional, nondimensional radial coordinate, $r = R/a$
r_1	radial location of the free surface at $z = 0$ (cylinder bottom wall)
r_2	radial location of the free surface at $z = 2\alpha$ (cylinder top wall)
Re	Reynolds number, $\Omega_f a^2/\nu$
r_i	radial location of the vertical free surface (see Eq. 6)
T, τ	dimensional, nondimensional time, $\tau = T\Omega_f$
U, u	dimensional, nondimensional radial velocity component, $u = U/\Omega_f a$
V, v	dimensional, nondimensional azimuthal velocity component, $v = V/\Omega_f a$
W, w	dimensional, nondimensional axial velocity component, $w = W/\Omega_f a$
Z, z	dimensional, nondimensional axial coordinate, $z = Z/a$
Z_i	liquid level at the cylinder spin axis for zero axial spin.
Z_o	liquid level at the cylinder spin axis for Ω_f spinrate.

Greek Symbols

α	cylinder aspect ratio, c/a
Γ, γ	dimensional, nondimensional circulation, $\gamma = \Gamma/\Omega_f a^2$
Δr	difference in free surface radial location between top and bottom cylinder walls, $r_2 - r_1$
Z, ζ	dimensional, nondimensional vorticity, $\zeta = Z/\Omega_f$
θ	azimuthal coordinate
μ	dynamic viscosity of the liquid fill
ν	kinematic viscosity of the liquid fill
ρ	density of the liquid fill
$\tau_{\theta r}$	tangential shear stress in the θ-direction on a surface with normal in the r-direction
τ_{zr}	tangential shear stress in the z-direction on a surface with normal in the r-direction
Ψ, ψ	dimensional, nondimensional stream function, $\psi = \Psi/\Omega_f a^3$
Ω_i	initial axial spinrate of the cylinder (rad/sec)
Ω_f	final or steady state axial spinrate of the cylinder (rad/sec)
Ω_f'	axial spinrate of the top wall of the cylinder (rad/sec)
ω	Gauss-Seidel relaxation parameter

Subscripts

r	first derivative with respect to the radial coordinate
rr	second derivative with respect to the radial coordinate
z	first derivative with respect to the axial coordinate
zz	second derivative with respect to the axial coordinate

Superscripts

k	current iteration
$k+1$	successive iteration

DISTRIBUTION LIST

No. of Copies	Organization
12	Administrator Defense Technical Information Center ATTN: DTIC-FDAC Cameron Station, Bldg. 5 Alexandria, VA 22304-6145
1	HQDA DAMA-ART-M Washington, DC 20310
1	Commander US Army Materiel Command ATTN: AMCDRA-ST 5001 Eisenhower Avenue Alexandria, VA 22333-0001
1	Commander US Army Armament RD&E Center ATTN: SMCAR-TDC Dover, NJ 07801-5001
1	Commander U.S. Army Armament RD&E Center US Army AMCCOM ATTN: SMCAR-MSI Dover, NJ 07801-5001
1	Commander U.S. Army Armament RD&E Center US Army AMCCOM ATTN: SMCAR-LC Dover, NJ 07801-5001
1	Commander U.S. Army Armament RD&E Center US Army AMCCOM ATTN: SMCAR-CAWS-AM Mr. Griggs Dover, NJ 07801-5001
1	OPM Nuclear ATTN: AMCPM-NUC Dover, NJ 07801-5001
1	AFWL/SUL Kirtland AFB,NM 87117-6008
4	Commander U.S. Army Armament RD&E Center US Army AMCCOM ATTN: SMCAR-AET-A Mr. R. Kline Mr. S. Kahn SMCAR-LCA-P Mr. F. Scerbo Mr. J. Bera Dover, NJ 07801-5001
1	Commander US Army Armament, Munitions and Chemical Command ATTN: AMSMC-IMP-L Rock Island, IL 61299-7300
1	Commander U.S. AMCCOM ARDEC CCAC Benet Weapons Laboratory ATTN: SMCAR-CCB-TL Watervliet, NY 12189-4050
1	Commander US Army Aviation Systems Command ATTN: AMSAV-ES 4300 Goodfellow Blvd St. Louis, MO 63120-1798
1	Director US Army Aviation Research and Technology Activity Ames Research Center Moffett Field, CA 94035-1099
1	Commander US Army Communications - Electronics Command ATTN: AMSEL-ED Fort Monmouth, NJ 07703-5000
1	Commander CECOM R&D Technical Library ATTN: AMSEL-IM-L, (Reports Section) B. 2700 Fort Monmouth, NJ 07703-5000

DISTRIBUTION LIST

No. of Copies	Organization
10	C. I. A. O.C/DB/Standard GE47 HQ Washington, DC 20505
1	Commandant US Army Infantry School ATTN: ATSH-CD-CS-OR Fort Benning, GA 31905-5400
1	Commander US Army Missile Command Research Development and Engineering Center ATTN: AMSMI-RD Redstone Arsenal, AL 35898-5230
1	Commander US Army Missile Command ATTN: AMSMI-RDK, Mr. R. Deep Redstone Arsenal, AL 35898-5230
1	Director US Army Missile and Space Intelligence Center ATTN: AIAMS-YDL Redstone Arsenal, AL 35898-5500
1	Commander US Army Tank Automotive Command ATTN: AMSTA-TSL Warren, MI 48397-5000
1	Director US Army TRADOC Analysis Center ATTN: ATOR-TSL White Sands Missile Range NM 88002-5502
1	Commander US Army Development & Employment Agency ATTN: MODE-ORO Fort Lewis, WA 98433-5000
1	Commandant US Army Field Artillery School ATTN: ATSF-GD Fort Sill, OK 73503
1	Director National Aeronautics and Space Administration Langley Research Center ATTN: Tech Library Langley Station Hampton, VA 23365
1	Director US Army Field Artillery Board ATTN: ATZR-BDW Fort Sill, OK 73503
1	Commander US Army Dugway Proving Ground ATTN: STEDP-MT Mr. G. C. Travers Dugway, UT 84022
1	Commander US Army Yuma Proving Ground ATTN: STEYP-MTW Yuma, AZ 85365-9103
2	Director Sandia National Laboratories ATTN: Dr. W. Oberkampf Dr. W. P. Wolfe Division 1636 Albuquerque, NM 87185
1	Air Force Armament Laboratory ATTN: AFATL/DLODL (Tech Info Center) Eglin AFB, FL 32542-5000
1	Hughes Aircraft ATTN: Dr. John McIntyre Mail Code S41/B323 P.O. Box 92919 Los Angeles, CA 90009

DISTRIBUTION LIST

No. of Copies	Organization
1	Aerospace Corporation Aero-Engineering Subdivision ATTN: Walter F. Reddall El Segundo, CA 90245
1	Carco Electronics 195 Constitution Drive Menlo Park, CA 94025
1	Commander Naval Surface Weapons Center ATTN: Dr. W. Yanta Aerodynamics Branch K-24, Building 402-12 White Oak Laboratory Silver Spring, MD 20910
1	Director National Aeronautics and Space Administration Marshall Space Flight Center ATTN: Dr. W. W. Fowlis Huntsville, AL 35812
1	Director National Aeronautics and Space Administration Ames Research Center ATTN: Dr. T. Steger Moffett Field, CA 94035
1	Calspan Corporation ATTN: W. Rae P.O. Box 400 Buffalo, NY 14225
2	Rockwell International Science Center ATTN: Dr. V. Shankar Dr. S. Chakravarthy 1049 Camino Dos Rios Thousand Oaks, CA 91360
1	University of Santa Clara Department of Physics ATTN: R. Greeley Santa Clara, CA 95053
1	Arizona State University Department of Mechanical and Energy Systems Engineering ATTN: G.P. Neitzel Tempe, AZ 85281
1	Massachusetts Institute of Technology ATTN: H. Greenspan 77 Massachusetts Avenue Cambridge, MA 02139
1	North Carolina State University Mechanical and Aerospace Engineering Department ATTN: F.F. DeJarnette Raleigh, NC 27607
1	Northwestern University Department of Engineering Science and Applied Mathematics ATTN: Dr. S.H. Davis Evanston, IL 60201
1	University of Colorado Department of Astro-Geophysics ATTN: E.R. Benton Boulder, CO 80302
2	Univeristy of Maryland ATTN: W. Melnik J.D. Anderson College Park, MD 20740
1	University of Maryland - Baltimore County Department of Mathematics ATTN: Dr. Y.M. Lynn 5401 Wilkens Avenue Baltimore, MD 21228
1	Rensselaer Polytechnic Institute Department of Math Sciences Troy, NY 12181

DISTRIBUTION LIST

No. of Copies	Organization
1	Director Lawrence Livermore National Laboratory ATTN: Mail Code L-35 Mr. T. Morgan P.O. Box 808 Livermore, CA 94550
1	University of Wisconsin-Madison Mathematics Research Center ATTN: Dr. John Strikwerda 610 Walnut Street Madison, WI 53706
2	Virginia Polytechnic Institute and State University Department of Aerospace Engineering ATTN: Tech Library Dr. Thorwald Herbert Blacksburg, VA 24061
1	University of Virginia Department of Mechanical Aerospace Engineering ATTN: W. E. Scott Charlottesville, VA 22904
1	University of California - Davis ATTN: Dr. Harry A. Dwyer Davis, CA 95616
1	Fluid Dynamics International, Incorporated ATTN: Dr. Simon Rosenblat 1600 Orrington Avenue Suite 505 Evanston, IL 60201
2	University of Maryland ATTN: E. Jones J. Vamos College Park, MD 20740

No. of Copies	Organization
	Aberdeen Proving Ground
	Director, USAMSAA ATTN: AMXSY-D
	Commander, USATECOM ATTN: AMSTE-TE-F, W. Vomocil
	PM-SMOKE, Bldg. 324 ATTN: AMCPM-SMK-M Mr. J. Callahan
	Cdr, CRDC, AMCCOM ATTN: SMCCR-MU Mr. W. Dee Mr. D. Bromley Mr. C. Hughes ATTN: SMCCR-RSP-A Mr. Miles Miller ATTN: SMCCR-SPS-IL SMCCR-RSP-A SMCCR-MU

USER EVALUATION SHEET/CHANGE OF ADDRESS

This Laboratory undertakes a continuing effort to improve the quality of the reports it publishes. Your comments/answers to the items/questions below will aid us in our efforts.

1. BRL Report Number _____ Date of Report _____

2. Date Report Received _____

3. Does this report satisfy a need? (Comment on purpose, related project, or other area of interest for which the report will be used.) _____

_____

_____

4. How specifically, is the report being used? (Information source, design data, procedure, source of ideas, etc.) _____

_____

_____

5. Has the information in this report led to any quantitative savings as far as man-hours or dollars saved, operating costs avoided or efficiencies achieved, etc? If so, please elaborate. _____

_____

_____

6. General Comments. What do you think should be changed to improve future reports? (Indicate changes to organization, technical content, format, etc.)

_____

_____

_____

CURRENT ADDRESS

_____
Name

_____
Organization

_____
Address

_____
City, State, Zip

7. If indicating a Change of Address or Address Correction, please provide the New or Correct Address in Block 6 above and the Old or Incorrect address below.

OLD ADDRESS

_____
Name

_____
Organization

_____
Address

_____
City, State, Zip

(Remove this sheet, fold as indicated, staple or tape closed, and mail.)

FOLD HERE

Director
US Army Ballistic Research Laboratory
ATTN: DRXBR-OD-ST
Aberdeen Proving Ground, MD 21005-5066

NO POSTAGE
NECESSARY
IF MAILED
IN THE
UNITED STATES

OFFICIAL BUSINESS
PENALTY FOR PRIVATE USE, $300

BUSINESS REPLY MAIL
FIRST CLASS PERMIT NO 12062 WASHINGTON, DC
POSTAGE WILL BE PAID BY DEPARTMENT OF THE ARMY

Director
US Army Ballistic Research Laboratory
ATTN: DRXBR-OD-ST
Aberdeen Proving Ground, MD 21005-9989

FOLD HERE